This is authors' accepted manuscript. Original article: https://doi.org/10.1152/ajpendo.00042.2020. Original article: Hydroxysteroid (17β) dehydrogenase 12 is essential for metabolic homeostasis in adult mice / Hanna Heikelä, Suvi T. Ruohonen, Marion Adam, Riikka Viitanen, Heidi Liljenbäck, Olli Eskola, Michael Gabriel, Laura Mairinoja, Alberto Pessia, Vidya Velagapudi, Anne Roivainen, Fu-Ping Zhang, Leena Strauss, and Matti Poutanen. Journal:
American Journal of Physiology-Endocrinology and Metabolism 2020 319:3, E494-E508

HYDROXYSTEROID (17β) DEHYDROGENASE 12 IS ESSENTIAL FOR THE METABOLIC HOMEOSTASIS IN ADULT MICE

Authors

Hanna Heikelä[1], Suvi T. Ruohonen[1], Marion Adam[1], Riikka Viitanen[2], Heidi Liljenbäck [1,2], Olli Eskola[2], Michael Gabriel[1], Laura Mairinoja[1], Alberto Pessia[3], Vidya Velagapudi[3], Anne Roivainen[1,2,4], Fu-Ping Zhang[1], Leena Strauss[1], Matti Poutanen[1,5]

Affiliations

[1]Turku Center for Disease Modeling, Institute of Biomedicine, University of Turku, Turku, Finland
[2]Turku PET Centre, University of Turku, Turku, Finland
[3]Institute for Molecular Medicine Finland, University of Helsinki, Helsinki, Finland
[4]Turku PET Centre, Turku University Hospital, Turku, Finland
[5]Department of Internal Medicine, Institute of Medicine, The Sahlgrenska Academy, University of Gothenburg, Sweden

Corresponding author

Matti Poutanen, Institute of Biomedicine, Research Centre for Integrative Physiology and Pharmacology, University of Turku, Kiinamyllynkatu 10, FI-20520 Turku, Finland, Phone +358-29-4502632, email: matti.poutanen@utu.fi

Author contributions

Hanna Heikelä: writing, experiment design, sample collection, data analysis
Suvi T. Ruohonen: experiment design, data analysis, sample collection
Marion Adam: mouse model generation
Riikka Viitanen: PET studies, writing
Heidi Liljenbäck: PET studies
Olli Eskola: PET studies
Michael Gabriel: image analysis, writing
Laura Mairinoja: image analysis
Vidya Velagapudi: lipidomics analysis
Alberto Pessia: lipidomics analysis
Anne Roivainen: PET studies, writing
Fu-Ping Zhang: mouse model generation
Leena Strauss: experiment design, writing
Matti Poutanen: experiment design, writing

Running head: HSD17B12 is essential for the metabolic homeostasis

ABBREVIATIONS

AA	arachidonic acid
Agrp	agouti-related peptide
ALT	alanine aminotransferase
BAT	brown adipose tissue
BSA	bovine serum albumin
CER	ceramide
Crh	corticotropin releasing hormone
CT	computed tomography
DCER	dihydroceramide
ESC	embryonic stem cells
FA	fatty acid
[^{18}F]FDG	2-[^{18}F]fluoro-2-deoxy-*D*-glucose
Flp	flippase
FRT	flippase recognition target
E	embryonic day
HCER	hexosylceramide
H&E	hematoxylin and eosin
HSD17B	hydroxysteroid 17-beta dehydrogenase
HSD17B12	hydroxysteroid 17-beta dehydrogenase type 12
KO	knockout
LCER	lactosylceramide
LPC	lysophosphatidylcholine
LPE	lysophosphatidylethanolamine
Npy	neuropeptide Y
PAS	periodic acid–Schiff
PC	phosphatidylcholine
Pomc	proopiomelanocortin
RCF	relative centrifugal force
SD	standard deviation
SDR	short-chain dehydrogenase/reductase
SM	sphingomyelin
SREBP	sterol regulatory element-binding protein
SUV	standardized uptake value
TAG	triacylglyceride
Tam	tamoxifen
TUNEL	terminal deoxynucleotidyl transferase dUTP nick end labeling
Veh	vehicle
WAT	white adipose tissue

ABSTRACT

Hydroxysteroid 17-beta dehydrogenase 12 (HSD17B12) is suggested to be involved in the elongation of very long chain fatty acids. Previously, we have shown a pivotal role for the enzyme during mouse development. In the present study we generated a conditional *Hsd17b12* knockout (HSD17B12cKO) mouse model by breeding mice homozygous for a floxed *Hsd17b12* allele with mice expressing the tamoxifen-inducible Cre recombinase at the ROSA26 locus. Gene inactivation was induced by administering tamoxifen to adult mice. The gene inactivation led to a 20% loss of body weight within six days, associated with drastic reduction in both white (83% males, 75% females) and brown (65% males, 60% females) fat, likely due to markedly reduced food and water intake. Furthermore, the knockout mice showed sickness behavior and signs of liver toxicity, specifically microvesicular hepatic steatosis and increased serum alanine aminotransferase (4.6-fold in males, 7.7-fold in females). The hepatic changes were more pronounced in females than males. Pro-inflammatory cytokines, such as interleukin 6 (IL-6), IL-17 and granulocyte-colony stimulating factor were increased in the HSD17B12cKO mice indicating inflammatory response. Serum lipidomics study showed an increase in the amount of dihydroceramides, despite the dramatic overall loss of lipids. In line with the proposed role for HSD17B12 in the fatty acid elongation, we observed accumulation of ceramides, dihydroceramides, hexosylceramides and lactosylceramides with shorter than 18-carbon fatty acid side chains in the serum. The results indicate that HSD17B12 is essential for proper lipid homeostasis, and HSD17B12 deficiency rapidly results in fatal systemic inflammation and lipolysis in adult mice.

Key words: liver, lipid, weight loss, toxicity, dihydroceramide

INTRODUCTION

Fourteen different hydroxysteroid 17-beta dehydrogenase (HSD17B) enzymes have been characterized as enzymes that have the ability to catalyze the reaction between 17-keto and 17-beta-hydroxy steroids, at least *in vitro*. HSD17Bs are encoded by different genes resulting in proteins with distinct amino acid sequences, and they present with different subcellular localizations as well as varying co-factor and substrate preferences [see review by (39)]. All, except HSD17B5, belong to the very large family of short-chain dehydrogenase/reductase (SDR) enzymes, known for their NAD(H)- or NADP(H)-dependent oxidoreductase activity. Several of the HSD17B enzymes are involved in the metabolism and synthesis of various lipids. For example, HSD17B4 is involved in the peroxisomal oxidation of fatty acids (7), while HSD17B8 has been suggested to have a role in the mitochondrial synthesis of fatty acids (10, 64), and HSD17B10 is capable for mitochondrial beta-oxidation of fatty acids (26). HSD17B7 is involved in *de novo* cholesterol synthesis (32), HSD17B12 is expected to be involved in long-chain fatty acid elongation (41) and HSD17B13 was recently shown to be a lipid droplet-associated protein (29) involved in lipid homeostasis in the liver (1).

HSD17B12 is widely expressed in both human and murine tissues (Fig. 1A, https://genevisible.com/tissues/HS/UniProt/Q53GQ0 and other expression data banks). The enzyme was originally characterized as an enzyme converting palmitic acid to arachidonic acid (AA) (41). The view that HSD17B12 is involved in fatty acid chain elongation is further supported by several studies. The enzyme expression was shown to be regulated by sterol regulatory element-binding protein (SREBP), a key regulator of several enzymes involved in lipid metabolism and fatty acid and cholesterol biosynthesis (42). Furthermore, knockdown of the *Hsd17b12* expression in cultured SK-BR-3 breast cancer cells resulted in reduced cell proliferation while the proliferation was restored by arachidonic acid treatment (43). Our *in vivo* study applying a mouse model with a hypomorphic *Hsd17b12* showed that a reduced expression of the gene in the ovaries resulted in failure in oogenesis and ovulation, and the phenotype was associated with a decrease in the intraovarian concentration of AA, and several of its downstream metabolites, including several prostaglandins (33). Similarly,

the amount of AA was decreased in embryonic stem cells (ESC) presenting only one functional copy of the gene (46).

Deleting the *Hsd17b12* gene from the mouse germ line resulted in early embryonic lethality at E9.5 at the latest (4, 46). A more detailed analysis of the knockout (KO) embryos revealed that the embryos initiate gastrulation, but their development was disrupted during early organogenesis, indicating that the *Hsd17b12* expression is essential for proper embryonic growth and differentiation. More recently, the fatty acid elongation by HSD17B12 has been shown to play a role in the development of inflammation and cancer (14, 34, 43, 66), and in line with these studies, HSD17B12 was also associated with a poor progression of ovarian cancer in a recent genome-wide association study (61). The role of HSD17B12 in ovarian cancer was also indicated by a genome-wide CRISPR/Cas screen of numerous cancer cell lines (3).

In the current study, we aimed to further characterize the *in vivo* function of HSD17B12 by generating *Hsd17b12* gene deletion at adulthood by utilizing the Cre-lox approach, allowing us to overcome the embryonic lethality observed in mice with the germ line deletion.

MATERIALS AND METHODS

Generation of mouse lines with conditional inactivation of HSD17B12

The targeting vector for HSD17B12 (PGS00030_C_C05) was obtained from the European Conditional Mouse Mutagenesis Program (EUCOMM). In the construct, exon 2 of *Hsd17b12* gene was flanked by *loxP* sites, and a *lacZ* as well as *neo* cassette was flanked by *FRT* sites. The vector was linearized, and electroporated into G4 hybrid mouse embryonic stem cells (G4, 129S6B6F1) for homologous recombination with standard procedures. To identify the properly targeted clones, the colonies were screened with specific primers for the wild type (wt) and the mutated allele (Table 1). The proper homologous recombination was then confirmed by sequencing. Thereafter, the *lacZ-neo* cassette was removed from the selected ES cell clones by Flp recombination, and the cells were injected into C57BL/6N mouse blastocysts. The blastocysts were then surgically transferred into pseudopregnant foster mothers (NMRI strain). The resulting chimeric offspring were genotyped, and mated with wt C57BL/6NCrl mice to produce the F1 generation to test the germ line transmission. The mouse colony was maintained by using the heterozygous littermates in breeding. A schematic representation of the targeted, floxed and deleted allele is shown in Supplemental Fig. S1A (All supplemental material is available at https://doi.org/10.6084/m9.figshare.12465512). The presence of the wt and/or mutated *Hsd17b12* gene in mice was analyzed by PCR (Table 1, Supplemental Fig. S1B). The mice with the floxed allele were crossed with Rosa26CreER^{T} strain (67) to generate a tamoxifen-inducible conditional KO mouse strain (HSD17B12cKO, Supplemental Fig. S1C). The primer pair used to identify the presence of Rosa26Cre-ER^{T} alleles is listed in Table 1. The adipocyte-specific, tamoxifen-inducible conditional KO mouse strain (aHSD17B12cKO, Supplemental Fig. S1D) was generated by breeding the HSD17B12-loxP with AdipoqCreER^{T2} mice (51). The primers used for genotyping the presence of Cre-ER^{T2} gene in these mice are shown in Table 1.

Gene deletions in both KO models were induced by daily intraperitoneal injections of 1.5 mg tamoxifen (Tam) (Sigma-Aldrich, Saint Louis, MO, USA) for five consecutive days. Tamoxifen was dissolved in ethanol and then diluted 1:10 in rapeseed oil. Ethanol diluted in rapeseed oil was used as a vehicle.

All animal handlings were conducted under the animal license number 10605/04.10.07/2016, granted by the Animal Experiment Board in Finland, and were carried out in accordance with the institutional animal care policies that fully meet the requirements defined in the National Institutes of Health (Bethesda, MD, USA) guidelines on animal experimentation. Animals were housed at the Central Animal Laboratory at the University of Turku, Finland, in individually ventilated cages (IVC, Techniplast, Buguggiate, Italy) with approximately 70 air changes per hour, and with constant temperature at 21 ± 3°C and humidity at 55 ± 15%. A 12:12h light:dark cycle was applied, with a light change at 7 am and 7 pm. Autoclaved aspen chips were used as bedding (Tapvei Ltd, Harjumaa, Estonia), and soy-free pellets (RM3, Special Diets Services, Essex, UK) and water were available *ad libitum.* Every cage had a nest-box and tissue paper was provided for nest building. The animals were individually identified with ear marks and housed with littermates (1-6 mice per cage). Animals were sacrificed with CO_2 asphyxiation and cervical dislocation.

Analyzing the body weight, body composition and weight of the adipose tissue depots

HSD17B12cKO: The body weight of the mice was monitored for seven days by weighing the mice once a day, starting at the time of the last Tam injection (day zero). The body composition (lean mass, fat mass, free water) was measured using the EchoMRI-700™ device (Echo Medical Systems, Houston, TX, USA) in live mice on day six after the last Tam injection. At the time of necropsy (six days after the last Tam injection) the weight of the various white adipose tissue (WAT) depots (subcutaneous, gonadal, perirenal), brown adipose tissue (BAT) as well as various organs (liver, spleen, kidneys, adrenals, pancreas, pituitary, heart) were measured and collected in liquid nitrogen and formalin.

aHSD17B12cKO: The body weight and composition of the mice were monitored for three months by weighing the mice and performing the EchoMRI analyses once a month. The mice were sacrificed at the age of five months and interscapular BAT, subcutaneous, gonadal and perirenal adipose tissue as well as liver were collected in liquid nitrogen and formalin.

Histological analysis

For hematoxylin and eosin (H&E) or Periodic acid–Schiff (PAS) staining, tissues collected at the time of necropsy were dissected and fixed in 10% buffered formalin at room temperature for 24-48h, dehydrated with increasing ethanol concentrations and xylene, and embedded in paraffin. After deparaffinization and rehydration, 4 µm-thick sections were stained with H&E or PAS for microscopic analysis. For Oil Red O (ORO) staining, the tissue samples were embedded in Tissue-Tek® O.C.T.^{TM} (Sakura Finetek USA, Inc., Torrance, CA, USA) and frozen in 2-methylbutane cooled with dry ice. Then 8 µm thick sections were cut and stained with ORO (Sigma-Aldrich). Microscope slides were scanned using Pannoramic 250 Flash digital slide scanner (3DHISTECH Ltd., Budapest, Hungary).

Quantification of apoptotic cells in the liver

Four micrometers thick paraffin sections of the liver from HSD17B12cKO and control mice (males CTRL n=7, KO=7; females CTRL n=6, KO=8) were deparaffinized and rehydrated. Antigen retrieval was performed in microwave in citrate buffer (pH 6.0). Endogenous peroxidase activity was inhibited by 3% H_2O_2. The sections were then incubated in the TUNEL reaction mixture containing TdT and biotin-16-dUTP (Roche Diagnostics GmbH) for 37°C for one hour. The reaction was terminated by adding 300 mM NaCl over the sections. The sections were then blocked with 3% BSA and incubated in ExtrAvidine (Sigma-Aldrich, diluted 1:500 in 1% BSA) for 30 min at 37°C, followed by staining with 3,3' diaminobenzidine (Dako Liquid DAB+ Substrate Choromogen System; Dako North America, Carpinteria, CA, USA). Finally, the sections were counterstained with Mayer's hematoxylin, dehydrated and mounted.

Slides were scanned using Pannoramic 250 Flash digital slide scanner (3DHISTECH Ltd., Budapest, Hungary). Digital slide images were then imported into QuPath, Version 0.2.0, an open-source software platform (2). Apoptotic cells were identified using the positive cell detection feature of QuPath, which detects the nuclei and classifies them as positive (apoptotic cells) or negative with QuPath's built-in cell segmentation algorithms. The analysis was performed on one sagittal section of the left lateral lobe per animal (mean area 52.2 mm^2). A total

of three outliers were excluded by ROUT method in GraphPad Prism (GraphPad Software, La Jolla, CA, USA) with coefficient Q=1% form male CTRL, male KO and female CTRL groups, one from each group. The mean percentage of positive nuclei of all detected nuclei was compared between the control and KO groups.

Adipocyte size

PAS-stained adipose tissue slides were scanned for further analysis with Pannoramic 250 Flash series digital slide scanner (3DHISTECH Ltd). Three to four 10x images were taken with the 3DHISTECH CaseViewer version 2.3. AdipoCount software (74) was used to measure the average adipocyte size in the images for each animal.

Triglyceride measurement

Frozen liver samples were homogenized in PBS containing 0.01% Nonidet P-40 (Roche Diagnostics GmbH) with TissueLyser LT (QIAGEN, Hilden, Germany) using 5 mm stainless steel beads at 50 Hz for 2 minutes. After homogenization, the samples were incubated on ice for 30 minutes and spun down for two minutes at 12000 RCF. Triglyceride concentration was measured in the supernatants with Serum Triglyceride Determination Kit (Sigma-Aldrich) according to manufacturer's instructions, scaled down for 96-well plates. The absorbance was measured with EnSight™ multimode plate reader (PerkinElmer, Waltham, MA, USA).

Analyzing the mRNA expression

RNA was extracted from frozen tissues with TRIsure™ (Bioline, London, UK) and treated with Amplification Grade DNase I (Sigma-Aldrich). One microgram of RNA was then reverse-transcribed using SensiFAST™ cDNA Synthesis Kit (Bioline), and mRNA levels were analyzed by quantitative RT-PCR using Dynamo Flash SYBR Green qPCR Kit (Thermo Fisher Scientific, Waltham, MA, USA) and the CFX96 Real-Time C1000 Thermal Cycler (Bio-Rad, Hercules, CA, USA). Standards were run in duplicates, and all the genes of interest as well as reference genes [ribosomal protein L19 (*L19*) and peptidylprolyl isomerase A (*Ppia*)] used for normalization were analyzed in triplicates. Sequences of the primers used are listed in Table 1.

Clinical chemistry analyses of the blood

Various clinical chemistry parameters were analyzed in seven control (Cre- lox/lox) and six HSD17B12cKO (Cre+ lox/lox) male mice as well as in five control (Cre- lox/lox) and five (Cre+ lox/lox) female mice on day six after the Tam induction. Approximately 110 µl of whole blood were collected from saphenous vein in BD Microtainer® lithium-heparin blood collection tubes (Becton, Dickinson and Company, Franklin Lakes, NJ, USA) and analyzed for albumin, alkaline phosphatase, alanine aminotransferase (ALT), amylase, blood urea nitrogen, total calcium, creatinine, globulin, glucose, potassium, sodium, phosphate, total bilirubin and total protein concentrations using Comprehensive Diagnostic Profile rotor (Abaxis, Inc., Union City, CA, USA) Vetscan VS2 analyzer (Abaxis, Inc.).

Lipidomics analysis in the serum

For lipidomic studies, blood was collected from five control (Cre-, lox/lox) and five HSD17B12cKO (Cre+, lox/lox) males, six days post Tam induction via heart puncture, allowed to coagulate overnight at +4°C and spun down to extract serum. Thereafter, quantitative lipidomic analysis was carried out as described earlier (23). Shortly, lipids were extracted with liquid-liquid extraction using ethyl acetate and methanol. To a 100 µl serum sample 1 ml methanol, 1 ml water and 100 µl of labelled internal lipid standards were added, and lipids were extracted by adding 3.5 ml of ethyl acetate. Dried samples were reconstituted with 250 µl of mobile phase (dichloromethane:methanol; 50:50, containing 10 mM ammonium acetate) for injection. Lipid separation and quantitation was performed on the SCIEX Lipidyzer™ platform using a SCIEX 5500 QTRAP® mass spectrometer (SCIEX, Framingham, MA, USA) with SelexION® Differential ion mobility (DMS) technology. The lipid molecular species were measured using MRM strategy in both positive and negative polarities. Positive ion mode was used for the detection of lipid classes dihydroceramides (DCER), hexosylceramides (HCER), lactosylceramides (LCER), sphingomyelins (SM), diacylglycerols (DAG), cholesteryl esters (CE), ceramides (CER), triacylglycerols (TAG), and negative ion mode was used for the detection of lipid classes lysophosphatidylethanolamines (LPE), lysophosphatidylcholines (LPC), phosphatidylcholines (PC), phosphatidylethanolamines (PE) and free fatty acids (FFA). Lipidomics Workflow Manager software (SCIEX)

was used for acquisition of samples, automated data-processing, signal detection and lipid species concentration calculations. Data analysis was performed with MetaboAnalyst 4.0 (11). A total of 856 lipids were analyzed, of which 222 lipids contained missing values. Of these, 137 lipids were found to have missing values in at least 40% of samples (2 samples) in both KO and control mice and were, therefore, discarded prior to the statistical analysis. Missing values from the remaining 85 lipids were imputed using MissForest package (60). Values were log-transformed, and no outliers were observed.

Measuring serum cytokines

Blood was collected via heart puncture from ten control (Cre-, lox/lox) and ten HSD17B12cKO (Cre+, lox/lox) males as well as nine control (Cre-, lox/lox) and ten HSD17B12cKO (Cre+, lox/lox) females on day six post Tam induction. To separate serum, blood was allowed to coagulate overnight at +4^{o}C and spun down. Cytokine levels were measured using Luminex 200 with xPONENT 3.1. software (Luminex, Austin, TX, USA) and MILLIPLEX MAP Mouse Cytokine/Chemokine Magnetic Bead Panel, MCYTOMAG-70K-PMX (Merck Millipore, Billerica,MA, USA) according to manufacturer's protocol. The cytokines measured included granulocyte-colony stimulating factor (G-CSF), Granulocyte-macrophage colony stimulating factor (GM-CSF), interferon gamma (IFN-y), interleukin 1 alpha (IL-1a), IL-1B, IL-2, IL-4, IL-5, IL-6, IL-7, IL-9, IL-10, IL-12 (p40), IL-12 (p70), IL-13, IL-15, IL-17, interferon gamma-induced protein 10 (IP-10), keratinocyte chemoattractant (KC), monocyte chemoattractant protein 1 (MCP-1), macrophage inflammatory protein 1-alpha (MIP-1a), MIP-1B, MIP-2, RANTES and tumor necrosis factor alpha (TNFa). The minimum detectable concentrations were 3.2 pg/ml for all the cytokines except 12.8 pg/ml for IL-13.

Indirect calorimetry

Six control (Cre- lox/lox) and six HSD17B12cKO (Cre+ lox/lox) males were placed (one mouse per cage) in OxyletPro™ indirect calorimetry cages (Panlab, S.L.U., Barcelona, Spain) three days after the first Tam injection. The system analyzes changes in O_2 and CO_2 concentrations and its high precision extensiometric weight transducer measures water consumption. In addition, the sensor platform records spontaneous activity and rearing

events to determine activity levels. The measurement (three days) was conducted between days three and five post Tam induction.

Measuring the food consumption

Three control (Cre- lox/lox) and five HSD17B12cKO (Cre+ lox/lox) males were housed in individual cages. To determine the amount of consumed food, food pellets were weighed before and after the measuring period in the morning of day zero (after the last Tam injection) and then every 24 hours until day five post Tam induction.

[^{18}F]FDG positron emission tomography (PET) studies

To standardize blood glucose level, mice were fasted for 3 h with *ad libitum* access to water prior to 2-[^{18}F]fluoro-2-deoxy-*D*-glucose ([^{18}F]FDG) injection. The blood glucose concentrations were measured using a glucometer (Bayer Contour, Bayer, Leverkusen, Germany) before and after [^{18}F]FDG PET/computed tomography (CT) imaging. For PET/CT imaging, the mice were anesthetized using isoflurane (3-4% induction and 1-2% maintenance) and the tail vein was cannulated. The mice were intravenously injected with 5.1 ± 0.1 MBq of [^{18}F]FDG and scanned using a small-animal PET/CT (Inveon Multimodality, Siemens Medical Solutions, Knoxville, TN, USA) for 60 minutes starting from the time of the injection. The PET data acquired in a list mode was iteratively reconstructed with an ordered subset expectation maximization 3D algorithm, followed by maximum a posteriori reconstruction. Quantitative PET image analysis was performed using Carimas 2.9 software (Turku PET Centre). The regions of interest were defined in brain, heart, kidney, liver, lung, muscle and urinary bladder using CT as the anatomical reference. The uptake of [^{18}F]FDG was reported as a standardized uptake value (SUV) which takes into account animal weight and injected radioactivity dose. Immediately after PET/CT, blood was collected via cardiac puncture under terminal isoflurane anesthesia and mice were sacrificed by cervical dislocation, various tissues were excised and weighted, and their total radioactivity was measured using a gamma counter (Triathler 3", Hidex Oy, Turku, Finland). The results were expressed as SUV.

Statistical analysis

Statistical analyses were carried out using GraphPad Prism 8.1.2 software (GraphPad Software, La Jolla, CA, USA). Outliers were identified using ROUT method in Prism with coefficient Q=1%. Shapiro-Wilk test was used to test for normal distribution. The statistical tests were chosen depending on the results of the Shapiro-Wilk tests of data normality. If not otherwise indicated, unpaired t test or nonparametric Mann-Whitney test was used to determine the statistical significance between two groups at single time point and two-way ANOVA for multiple time points. For adipocyte size and *Hsd17b12* mRNA expression, the statistical significance was analyzed by one-way ANOVA. The threshold for statistical significance was set at $p<0.05$. Results were expressed as mean ± standard deviation (SD), unless otherwise indicated.

Supplemental Figures are available at https://doi.org/10.6084/m9.figshare.12465512

RESULTS

Inducing HSD17B12 gene inactivation in adulthood results in dramatic weight loss

In the HSD17B12cKO mouse model, the exon 2 deletion was initiated at the age of eight weeks by injecting 1.5 mg of Tam/day for five consecutive days. This resulted in a marked decrease in *Hsd17b12* mRNA levels in the different tissues measured six days after Tam injection, while with vehicle injection no effect on the mRNA expression was observed (Fig. 1A). This confirmed the Tam-dependency of the gene deletion. The strongest reduction in the mRNA level was observed in the liver with a drop of 94%, followed by the colon (85%), the WAT (77%) and BAT (76%). Also in the kidney (50%) and spleen (56%) a significant reduction was observed. In the different brain regions and adrenals the mRNA levels were not reduced significantly six days after completing the Tam treatment (Fig. 1A), despite the confirmed expression of tamoxifen-inducible Cre-recombinase. The reason for phenotyping the mice only six days after the initiation of the gene deletion was due to the fact that both the male and female HSD17B12cKO mice were dramatically losing body weight during these 6 days (Fig. 1B), and at day 6 the weight was reduced 17% in males (KO day zero, 30.3 g ± 1.45 g; KO day six, 25.1 ± 3.17 g) and 24% in females (KO day zero, 23.2 g ± 0.95 g; KO day six, 18.1 g ± 1.59 g). No effect on body weight during the study period was observed in the Tam-treated controls lacking the Cre or expressing one wt allele. The weight loss was especially severe from day four to six. The physical appearance and behavior of the HSD17B12cKO mice were normal until day six, while at day six the mice sat hunched and showed other signs of general indisposition, and thus, the study period could not be extended. As analyzed by EchoMRI, the weight loss was accompanied with drastically lower fat content in the HSD17B12cKO mice compared with the Tam-treated controls in both females and males (56% and 66% lower, respectively, Fig. 1C). The reduced fat mass was confirmed *ex vivo* by analyzing the weights of the different adipose tissue depots (Supplemental Fig. S2). The reduced amount of fat in the HSD17B12cKO mice was also associated with reduced lipid droplet size in both the WAT and BAT in HSD17B12cKO mice compared with controls (Fig. 1D). The loss of fat tissue was accompanied by a significant loss of the lean mass (23% in females and 25% in males).

The weight loss in HSD17B12cKO mice is caused by reduced water and food intake, while the hypothalamic regulation of feeding is intact

To define the cause of the rapid loss of adipose tissue, we first assessed the overall energy consumption of HSD17B12cKO males. The data indicated that energy consumption of the HSD17B12cKO did not differ from that of the control mice when normalized to the lean mass (Supplemental Fig. S3A). Therefore, the results indicate that the weight loss was not primarily due to an increased metabolic rate of the HSD17B12cKO mice. Neither was there a difference in the locomotor activity (Supplemental Fig. S3B) or in the number of rearing events (Supplemental Fig. S3C) between the HSD17B12cKO and the control mice. However, HSD17B12cKO males show a decreased respiratory exchange ratio during day four, indicating a switch from using carbohydrates as the fuel source to burn fat (Supplemental Fig. S3D). While measuring the water and food intake we observed that the HSD17B12cKO mice drastically reduced water consumption during the days three to five after Tam induction (Fig. 2A), as well as the caloric intake was markedly reduced during the days two to five post induction (Fig. 2B). The control males consumed 3.7-4.0 g of chow per day while the HSD17B12cKO males consumed only 0.4-1.4 g per day, resulting in significantly reduced food consumption over the study period ($p< 0.004$), also indicated by lower serum glucose levels in KO mice compared to controls (Table 2). Increased levels of serum albumin and total proteins in HSD17B12cKO compared with the controls, measured on day six post induction, indicated severe dehydration of HSD17BcKO mice (Table 2). The lipid contents in the feces of KO mice did not differ from that of the control mice, suggesting that the weight loss was not due to fat malabsorption in the KO mice (Fig. 2C). These data prompted us to assess the expression levels of the genes mediating the satiety and hunger signals in the hypothalamus. mRNAs for major hunger-inducing signaling components, such as neuropeptide Y (*Npy*) and agouti-related peptide (*Agrp*) were upregulated, while for those regulating satiety, proopiomelanocortin (*Pomc*) was downregulated and corticotropin releasing hormone (*Crh*), was upregulated in the HSD17B12cKO mice compared with the control mice (Fig. 2D). Using [^{18}F]FDG PET imaging, both *in vivo* and *ex vivo* results (Supplemental Fig. S4) indicated a normal, or slightly increased, glucose uptake in the brain of HSD17B12cKO

mice compared with the controls. These results suggest that the hypothalamic regulation of feeding is responsive to the weight loss condition, and that the observed metabolic defect is not of hypothalamic origin.

HSD17B12 expression in the adipocytes is not essential for the metabolic homeostasis

We also investigated whether the significantly reduced HSD17B12 expression detected in the adipose tissue of the HSD17B12cKO (Fig. 1A) initiates the observed metabolic disturbance. For this purpose, we generated an inducible adipocyte-specific HSD17B12 KO mouse model (aHSD17B12cKO). The gene deletion in the adipocytes was induced by a 5-day-long Tam treatment at the age of eight weeks, followed by the analysis of body weight and body composition of the mice. However, within six days after Tam treatment no alteration in body weight or fat content was observed. Neither did we observe a phenotype similar to that of the HSD17B12cKO mice at any of the later time points, despite a marked decrease in *Hsd17b12* mRNA expression in the adipocytes (Fig. 3A). Three months after the Tam injection, the aHSD17B12cKO mice presented with a body fat mass and lean mass similar to those of the control mice (Fig. 3B-D). Furthermore, the lipid droplets within adipocytes did not appear smaller in the aHSD17B12cKO mice than in the control mice (Fig. 3E). These results indicated that the loss of HSD17B12 activity in the adipocytes in adult mice does not lead to the severe metabolic alteration and starvation that was observed in the HSD17B12cKO mice.

Inducing HSD17B12 gene inactivation at adulthood results in altered serum lipid profile, liver steatosis and signs of general toxicity

We next performed serum lipidomic analysis to obtain a more detailed understanding of the consequences of the *Hsd17b12* disruption on circulating lipids in HSD17B12cKO mice. As expected, and shown by the heat map (Fig. 4A), the majority of the 872 metabolites of 13 different lipid classes measured were at markedly lower levels in the HSD17B12cKO mice, while some lipid species accumulating in the KO mice were identified as well. The genotypes completely segregated into separate clusters according to the phenotype. The Volcano-plot (Fig. 4B) shows that TAG was the most severely decreased lipid class, but also CER, LPE, LPC, PC, SM and LCER were significantly decreased in HSD17B12cKO serum compared to controls. Interestingly, the HSD17B12cKO

showed a 1.39 fold higher concentration of DCER ($log_2(1.39) = 0.48$) Fig. 4B) compared to controls, being the only lipid class found to accumulate during the weight loss. As the total amount of ceramides was markedly reduced, the DCER/CER ratio was increased by 2.6-fold (CTRL, DCER/CER = 0.16; KO, DCER/CER =0.42), with highest increase in the concentration of DCER (FA16:0). In all groups of ceramides (CER, DCER, LCER and HCER), we also observed increased relative amount of fatty acids with chain length of 14 and 16 carbon atoms (FA 14:0 and FA16:0), and a reduced amount of fatty acids with longer chain lengths (FA 18:0 and FA20:0, FA22:0 and 22:1, FA24:0 and 24:1, Fig. 4C). This strongly suggests a defect in the fatty acid elongation in the HSD17B12cKO. To our surprise, we did not observe any specific changes in the AA levels as a free form, or as a component of the various lipid classes.

Six days after the Tam injection we observed significant fat accumulation in the livers of female HSD17B12cKO mice (Fig. 5A,C). Fat accumulation was observed in some HSD17B12cKO male mice as well, but the difference in the amount of triglycerides between the control males and HSD17B12cKO males did not reach statistical significance. The liver injury in HSD17B12cKO mice was further supported by an 8-fold ($p< 0.005$) and a 5-fold increased serum ALT levels in HSD17B12cKO females and males, respectively, compared with control mice (Fig. 5B). In females, microvesicular steatosis was associated with a trend of increasing percentage of apoptotic cells in the HSD17B12cKO livers, indicating lipotoxic hepatocellular injury as well (Fig. 5D).

As the HSD17B12cKO mice showed signs of general toxicity and chronic pain with distress presented with piloerection, social isolation, partially closed eyelids, unresponsiveness and snout grooming, we measured cytokines in serum to analyze their general inflammatory status. The data revealed a marked increase in IL-6, IL-17 and G-CSF levels in both male and female KO mice compared to the controls (Table 3.). In addition, the data indicated a minor decrease in the levels of IP-10, IL-1a and IL-5 in males, and of MIP-1a, IFN-g and KC in females. These results further confirmed that the HSD17B12cKO mice suffered from systemic inflammation.

Energy depletion leads to reduced hepatic *de novo* lipogenesis and increased gluconeogenesis in HSD17B12cKO mice

The analysis of mRNA expression in liver samples of male mice six days after Tam induction did not indicate an enhanced FA uptake, as the mRNAs for the cluster of differentiation 36 (*Cd36*) and the fatty acid transport protein 2 (*Fatp2*) were not altered (Supplemental Fig. S5). Neither was there a difference in the mRNAs for the proteins centrally involved in FA oxidation between the control and HSD17B12cKO mice. Those measured included peroxisome proliferator-activated receptor alpha (*Ppara*), carnitine palmitoyl transferase 1 (*Cpt1a*) and acyl-CoA oxidase 1 (*Acox1*). However, of the mRNAs coding for the enzymes involved in FA esterification, diacylglycerol O-acyltransferase 1 (*Dgat1*) presented with a trend of higher expression in the HSD17B12cKO than in the control animals, while the mRNAs of key enzymes involved in *de novo* lipogenesis, such as acetyl-CoA Carboxylase alpha (*Acaca*), fatty acid synthase (*Fasn*) and Acyl-CoA desaturase 1 (*Scd1*)] were decreased in the HSD17B12cKO mice compared with the controls.

PAS staining of liver sections six days after Tam induction showed reduced glycogen contents in the HSD17B12cKO livers compared with control livers. As a compensatory effect, mRNA expression for the enzyme presenting the rate limiting step in gluconeogenesis, namely phosphoenolpyruvate carboxykinase (*Pepck*), was significantly increased in the HSD17B12cKO mice, and mRNA for *Pkrl*, which encodes for a pyruvate kinase was decreased in the KO animals. These results show that the hepatic glycogen storages of HSD17B12cKO mice were depleted six days after knockout induction, and that the lipids accumulating within the hepatocytes were not of hepatic origin.

DISCUSSION

In the present study, we generated an inducible conditional HSD17B12 KO mouse by crossing the HSD17B12-loxP mice with mice expressing tamoxifen-inducible Cre recombinase under the ubiquitously expressed *Rosa26* locus. Our previous studies showed that HSD17B12 is essential for mouse embryonic development (46). In the current study, we showed that HSD17B12 activity is also essential for normal metabolic homeostasis in adult mice. The disruption of the HSD17B12 action led to a drastic loss of body weight within six days post induction, evidenced by reduced fat and lean mass as well as severe dehydration. The weight loss was not observed in the adipocyte-specific HSD17B12cKO mouse model, indicating that, despite the high expression of *Hsd17b12* in murine fat, the loss of storage fat was not due to disrupted HSD17B12 function in the adipose tissue.

During the first five days after tamoxifen induction the general wellbeing of HSD17B12cKO mice appears normal, apart from weight loss. On the day six, we observed hunched posture, closed eyelids and reduced locomotor activity, which all are signs of general illness and pain (8, 17, 18), and no studies beyond day six post induction were warranted. Similar signs are often observed in mouse models of sepsis (56) and in pathogen-induced sickness (35), as well as during cytotoxic chemotherapy (19, 48). The HSD17B12cKO mice seemed to have a trend of decreased locomotor activity already between the days three and five, but the difference observed was not significant. Furthermore, the HSD17B12cKO mice showed microsteatosis and increased triglyceride accumulation in the liver together with increased plasma ALT levels, which all are indicators of liver injury (6, 37, 68), [for review (55)]. Female mice are known to be more sensitive to toxicity compared to males (30, 31, 59). This is in line with the higher serum ALT levels in HSD17B12cKO females compared to the KO males. There was also a trend for an increased apoptosis in female livers, but not in male livers. Thus, various indicative parameters for general wellbeing indicate that the mice with disrupted HSD17B12 enzyme suffer from general toxicity likely due to accumulation of toxic intermediates originating from the disrupted lipid metabolism.

The data indicated an increased level of pro-inflammatory cytokines, such as IL-6, IL-17 and G-CSF in the HSD17B12cKO mice. IL-6 has been shown to induce cachexia by increasing lipolysis in WAT (25, 70).

Furthermore, elevated serum IL-6 has been linked to weight loss in both cancer cachexia (54) and anorexia nervosa patients (15, 16). Thus, increased IL-6 is one potential mechanism for the weight loss observed in the HSD17B12cKO mice. The reduced lean mass and reduced glucose uptake in muscles in the HSD17B12cKO animals could be explained by elevated IL-6 as well, as high IL-6 has been shown to induce muscle atrophy in animal models of cachexia [for review (18)]. It is still unclear how the lack of HSD17B12 leads to an increase in the proinflammatory cytokines. However, our previous studies showed that disruption of HSD17B12 in mice leads to lower levels of prostanoids (PGD2, PGE2 PGF2a and TXB2) in ovaries (33). Prostanoids are involved in the regulation of cytokine production [for review (63)] and low levels of prostaglandin E2 has been shown to increase IL-17 levels (49), and increased IL-17, in turn, is capable of inducing both IL-6 and G-CSF (12, 71), consequently promoting inflammation and sickness behavior.

HSD17B12 deficiency drastically reduced water and food intake in three days. Thus, the weight loss observed in HSD17B12cKO mice could be explained by the reduced food and water intake. Similarly, a fast for 48h is sufficient to produce a weight loss up to 20% of body weight in mice (20). Moreover, we did not observe any changes in the whole body energy expenditure in the KO mouse, suggesting their general metabolism is not activated over that of the control mice. In a fasting state, the hypothalamic orexigenic peptide expressions of *Npy* and *Agrp* are known to increase, while anorexigenic *Pomc* mRNA is known to decrease in order to increase food intake and replenish the energy storages (9, 13, 24, 50, 52, 53), and accordingly, this was also observed in HSD17B12cKO mice six days post induction. This indicates that the hypothalamic regulation of hunger and satiety was responding to starvation in the HSD17B12cKO mice. Surprisingly, the *Hsd17b12* gene was still expressed in the brain, indicating that the 6-day-long time period following the Tam injection was not sufficient to induce the Cre-mediated recombination in the brain. However, the anorexigenic *Crh* expression was increased in the KO mice. *Crh* is also a major regulator of stress response (27) and administration of CRH is known to suppress appetite, and cause anorexia in mice (5, 21, 62). Thus, the increased *Crh* expression in HSD17B12cKO mice in adulthood is in line with the observed stress response in the mice and, in addition to IL-6, could inhibit food intake.

In line with the heavily reduced adipose mass, serum lipid concentrations were mostly reduced in the HSD17B12cKO mice compared to controls. However, we surprisingly observed an increased concentration of dihydroceramides in our KO model. Recent studies have found dihydroceramides as regulators of autophagy in cell culture models of hepatic steatosis and cancer (28, 36). Furthermore, an increased ratio of dihydroceramides:ceramides has been shown to mediate apoptosis (28), and starvation is also known to induce autophagy (44, 47, 72). Thus, the increased dihydroceramide levels in HSD17B12cKO could contribute to the observed liver steatosis and inflammation. The lipidomics data also revealed a proportional increase in FA16 containing lipids in the HSD17B12cKO mice with an equivalent decrease in lipids including longer fatty acids (FA18, FA20, FA22, FA24). This was also observed in cholesteryl esters, and to some extent in SM (short ones accumulate, long ones did not change), but this proportional increase in shorter fatty acids was not observed in the FFA, LPC, LPE, PC, PE or TAG classes. Together, this data suggests that HSD17B12 is essential for the normal composition of sphingomyelins and their precursors, *i.e.* ceramides and dihydroceramides.

Due to their heavily reduced food intake, the metabolic state of HSD17B12cKO mice at least partially resembles that of prolonged fasting. *De novo* lipogenesis appeared to be decreased, while gluconeogenesis was increased in the HSD17B12cKO mice, in line with previous studies on fasting response (40, 57). Defects in FA oxidation is a common cause behind fat accumulation in the hepatocytes in NAFLD [for review (38)]. However, this does not seem to be the mechanism for liver steatosis in the HSD17B12cKO mice. Of the other enzymes studied, DGAT1 preferably esterifies FAs imported to the cell, while DGAT2 utilizes FAs originating from *de novo* lipogenesis. Thus, the observed trend of induced *Dgat1* expression in the liver without a change in the *Dgat2* expression supports the idea of increased fat mobilization from adipose tissue in the HSD17B12cKO mice (45, 65, 69).

In conclusion, our KO mouse data show that *Hsd17b12* is essential for metabolic homeostasis in adult mice, and *Hsd17b12* gene disruption leads to severe weight loss and liver steatosis. Mice with disrupted HSD17B12 enzyme suffer from general toxicity, possibly due to accumulation of toxic intermediates originating from the disrupted lipid metabolism or an imbalance in the production of prostaglandins and cytokines, leading to cytokine-induced

sickness behavior. We suggest that the drastic loss of adipose tissue is largely due to an anorexia phenotype, potentially induced by the accumulation of toxic lipids. Further studies are needed to investigate the detailed mechanisms behind the severe inflammation and disrupted lipid homeostasis.

ACKNOWLEDGEMENTS

The authors would like to thank the personnel of Turku Center for Disease Modeling (www.TCDM.fi) and the Histology Core Facility at Institute of Biomedicine, University of Turku, Turku PET Centre and the Central Animal Laboratory, at University of Turku, as well as the personnel of the Metabolomics Unit, Technology Centre, Institute for Molecular Medicine Finland (FIMM), at the University of Helsinki for assistance. Turku Center for Disease Modeling is part of the Biocenter Finland Model Organisms Infrastructure. This work was financially supported by Sigrid Jusélius Foundation, the Academy of Finland, Novo Nordisk Foundation and Finnish Cultural Foundation.

REFERENCES

1. **Adam M**, **Heikelä H**, **Sobolewski C**, **Portius D**, **Mäki-Jouppila J**, **Mehmood A**, **Adhikari P**, **Esposito I**, **Elo LL**, **Zhang F-P**, **Ruohonen ST**, **Strauss L**, **Foti M**, **Poutanen M**. Hydroxysteroid (17β) dehydrogenase 13 deficiency triggers hepatic steatosis and inflammation in mice. *FASEB J* 0: fj.201700914R, 2018.

2. **Bankhead P**, **Loughrey MB**, **Fernández JA**, **Dombrowski Y**, **McArt DG**, **Dunne PD**, **McQuaid S**, **Gray RT**, **Murray LJ**, **Coleman HG**, **James JA**, **Salto-Tellez M**, **Hamilton PW**. QuPath: Open source software for digital pathology image analysis. *Sci Rep* 7: 1–7, 2017.

3. **Behan FM**, **Iorio F**, **Picco G**, **Gonçalves E**, **Beaver CM**, **Migliardi G**, **Santos R**, **Rao Y**, **Sassi F**, **Pinnelli M**, **Ansari R**, **Harper S**, **Jackson DA**, **McRae R**, **Pooley R**, **Wilkinson P**, **van der Meer D**, **Dow D**, **Buser-Doepner C**, **Bertotti A**, **Trusolino L**, **Stronach EA**, **Saez-Rodriguez J**, **Yusa K**, **Garnett MJ**. Prioritization of cancer therapeutic targets using CRISPR–Cas9 screens. *Nature* 568: 511–516, 2019.

4. **Bellemare V**, **Phaneuf D**, **Luu-The V**. Target deletion of the bifunctional type 12 17β-hydroxysteroid dehydrogenase in mice results in reduction of androgen and estrogen levels in heterozygotes and embryonic lethality in homozygotes. *Horm Mol Biol Clin Investig* 2: 311–318, 2010.

5. **Benoit SC**, **Thiele TE**, **Heinrichs SC**, **Rushing PA**, **Blake KA**, **Steeley RJ**. Comparison of central administration of corticotropin-releasing hormone and urocortin on food intake, conditioned taste aversion, and c-Fos expression. *Peptides* 21: 345–351, 2000.

6. **Bernhard A**, **Rasinger JD**, **Wisløff H**, **Kolbjørnsen Ø**, **Secher Myrmel L**, **Berntssen MHG**, **Lundebye AK**, **Ørnsrud R**, **Madsen L**. Subchronic dietary exposure to ethoxyquin dimer induces microvesicular steatosis in male BALB/c mice. *Food Chem Toxicol* 118: 608–625, 2018.

7. **Breitling R**, **Marijanović Z**, **Perović D**, **Adamski J**. Evolution of 17beta-HSD type 4, a multifunctional protein of beta-oxidation. *Mol Cell Endocrinol* 171: 205–10, 2001.

8. **Burkholder T**, **Foltz C**, **Karlsson E**, **Linton GC**, **Smith JM**. Health Evaluation of Experimental Laboratory Mice. *Curr Protoc Mouse Biol* 2: 145–165, 2012.

9. **Chen SR**, **Chen H**, **Zhou JJ**, **Pradhan G**, **Sun Y**, **Pan HL**, **Li DP**. Ghrelin receptors mediate ghrelin-induced excitation of agouti-related protein/neuropeptide Y but not pro-opiomelanocortin neurons. *J Neurochem* 142: 512–520, 2017.

10. **Chen Z**, **Kastaniotis AJ**, **Miinalainen IJ**, **Rajaram V**, **Wierenga RK**, **Hiltunen JK**. 17β-Hydroxysteroid dehydrogenase type 8 and carbonyl reductase type 4 assemble as a ketoacyl reductase of human mitochondrial FAS. *FASEB J* 23: 3682–3691, 2009.

11. **Chong J**, **Soufan O**, **Li C**, **Caraus I**, **Li S**, **Bourque G**, **Wishart DS**, **Xia J**. MetaboAnalyst 4.0: Towards more transparent and integrative metabolomics analysis. *Nucleic Acids Res* 46: W486–W494, 2018.

12. **Chung AS**, **Wu X**, **Zhuang G**, **Ngu H**, **Kasman I**, **Zhang J**, **Vernes JM**, **Jiang Z**, **Meng YG**, **Peale F V.**, **Ouyang W**, **Ferrara N**. An interleukin-17-mediated paracrine network promotes tumor resistance to anti-angiogenic therapy. *Nat Med* 19: 1114–1123, 2013.

13. **Cowley MA**, **Smith RG**, **Diano S**, **Tschöp M**, **Pronchuk N**, **Grove KL**, **Strasburger CJ**, **Bidlingmaier M**, **Esterman M**, **Heiman ML**, **Garcia-Segura LM**, **Nillni EA**, **Mendez P**, **Low MJ**,

Sotonyi P, **Friedman JM**, **Liu H**, **Pinto S**, **Colmers WF**, **Cone RD**, **Horvath TL**. The distribution and mechanism of action of ghrelin in the CNS demonstrates a novel hypothalamic circuit regulating energy homeostasis. *Neuron* 37: 649–661, 2003.

14. **Dai W**, **Liu H**, **Xu X**, **Ge J**, **Luo S**, **Zhu D**, **Amos CI**, **Fang S**, **Lee JE**, **Li X**, **Nan H**, **Li C**, **Wei Q**. Genetic variants in ELOVL2 and HSD17B12 predict melanoma-specific survival. *Int. J. Cancer* (2019). doi: 10.1002/ijc.32194.

15. **Dalton B**, **Bartholdy S**, **Robinson L**, **Solmi M**, **Ibrahim MAA**, **Breen G**, **Schmidt U**, **Himmerich H**. A meta-analysis of cytokine concentrations in eating disorders. *J Psychiatr Res* 103: 252–264, 2018.

16. **Dalton B**, **Leppanen J**, **Campbell IC**, **Chung R**, **Breen G**, **Schmidt U**, **Himmerich H**. A longitudinal analysis of cytokines in anorexia nervosa. *Brain Behav Immun* 85: 88–95, 2020.

17. **Dantzer R**. Cytokine, Sickness Behavior, and Depression. *Immunol Allergy Clin North Am* 29: 247–264, 2009.

18. **Dantzer R**, **Kelley KW**. Twenty years of research on cytokine-induced sickness behavior. *Brain Behav Immun* 21: 153–160, 2007.

19. **Elsea CR**, **Kneiss JA**, **Wood LJ**. Induction of IL-6 by Cytotoxic Chemotherapy Is Associated With Loss of Lean Body and Fat Mass in Tumor-free Female Mice. *Biol Res Nurs* 17: 549–557, 2015.

20. **Enginar N**, **Nurten A**, **Türkmen AZ**, **Çağla B**. Scopolamine-induced convulsions in fasted animals after food intake: Sensitivity of C57BL/6J mice and Sprague-Dawley rats. *Epilepsy Res* 112: 150–153, 2015.

21. **Fatima A**, **Andrabi S**, **Wolf G**, **Engelmann M**, **Spina MG**. Urocortin 1 administered into the hypothalamic supraoptic nucleus inhibits food intake in freely fed and food-deprived rats. *Amino Acids* 44: 879–885, 2013.

22. **Friedrich G**, **Soriano P**. Promoter traps in embryonic stem cells: A genetic screen to identify and mutate developmental genes in mice. *Genes Dev* 5: 1513–1523, 1991.

23. **Gaiser RA**, **Pessia A**, **Ateeb Z**, **Davanian H**, **Fernández Moro C**, **Alkharaan H**, **Healy K**, **Ghazi S**, **Arnelo U**, **Valente R**, **Velagapudi V**, **Sällberg Chen M**, **Del Chiaro M**. Integrated targeted metabolomic and lipidomic analysis: A novel approach to classifying early cystic precursors to invasive pancreatic cancer. *Sci Rep* 9: 1–12, 2019.

24. **Hahn TM**, **Breininger JF**, **Baskin DG**, **Schwartz MW**. Coexpression of Agrp and NPY in fasting-activated hypothalamic neurons. *Nat Neurosci* 1: 271–272, 1998.

25. **Han J**, **Meng Q**, **Shen L**, **Wu G**. Interleukin-6 induces fat loss in cancer cachexia by promoting white adipose tissue lipolysis and browning. *Lipids Health Dis* 17: 1–8, 2018.

26. **He X**, **Merz G**, **Mehta P**, **Schulz H**, **Yang S**. Human Brain Short Chain L -3-Hydroxyacyl Coenzyme A Dehydrogenase Is a Single-domain Multifunctional Enzyme. *Biochemistry* 274: 15014–15019, 1999.

27. **Herman JP**, **Mcklveen JM**, **Ghosal S**, **Kopp B**, **Wulsin A**, **Makinson R**, **Scheimann J**, **Myers B**. Regulation of the hypothalamic-pituitary-adrenocortical stress response. Comprehensive Physiology. *Compr Physiol* 6: 603–621, 2016.

28. **Hernández-Tiedra S**, **Fabriàs G**, **Dávila D**, **Salanueva ÍJ**, **Casas J**, **Montes LR**, **Antón Z**, **García-Taboada E**, **Salazar-Roa M**, **Lorente M**, **Nylandsted J**, **Armstrong J**, **López-Valero I**, **McKee CS**,

Serrano-Puebla A, **García-López R**, **González-Martínez J**, **Abad JL**, **Hanada K**, **Boya P**, **Goñi F**, **Guzmán M**, **Lovat P**, **Jäättelä M**, **Alonso A**, **Velasco G**. Dihydroceramide accumulation mediates cytotoxic autophagy of cancer cells via autolysosome destabilization. *Autophagy* 12: 2213–2229, 2016.

29. **Horiguchi Y**, **Araki M**, **Motojima K**. 17β-Hydroxysteroid dehydrogenase type 13 is a liver-specific lipid droplet-associated protein. *Biochem Biophys Res Commun* 370: 235–238, 2008.

30. **Iimuro Y**, **Frankenberg M V.**, **Arteel GE**, **Bradford BU**, **Wall CA**, **Thurman RG**. Female rats exhibit greater susceptibility to early alcohol-induced liver injury than males. *Am J Physiol - Gastrointest Liver Physiol* 272, 1997.

31. **Ikejima K**, **Enomoto N**, **Iimuro Y**, **Ikejima A**, **Fang D**, **Xu J**, **Forman DT**, **Brenner DA**, **Thurman RG**. Estrogen increases sensitivity of hepatic Kupffer cells to endotoxin. *Am J Physiol - Gastrointest Liver Physiol* 274: 669–676, 1998.

32. **Jokela H**, **Rantakari P**, **Lamminen T**, **Strauss L**, **Ola R**, **Mutka AL**, **Gylling H**, **Miettinen T**, **Pakarinen P**, **Sainio K**, **Poutanen M**. Hydroxysteroid (17β) dehydrogenase 7 activity is essential for fetal de novo cholesterol synthesis and for neuroectodermal survival and cardiovascular differentiation in early mouse embryos. *Endocrinology* 151: 1884–1892, 2010.

33. **Kemiläinen H**, **Adam M**, **Mäki-Jouppila J**, **Damdimopoulou P**, **Damdimopoulos AE**, **Kere J**, **Hovatta O**, **Laajala TD**, **Aittokallio T**, **Adamski J**, **Ryberg H**, **Ohlsson C**, **Strauss L**, **Poutanen M**. The hydroxysteroid (17β) dehydrogenase family gene HSD17B12 is involved in the prostaglandin synthesis pathway, the ovarian function, and regulation of fertility. *Endocrinology* 157: 3719–3730, 2016.

34. **Kemiläinen H**, **Huhtinen K**, **Auranen A**, **Carpén O**, **Strauss L**, **Poutanen M**. The Expression of HSD17B12 Is Associated with COX-2 Expression and Is Increased in High-Grade Epithelial Ovarian Cancer. *Oncology* 94: 233–242, 2018.

35. **Kolmogorova D**, **Murray E**, **Ismail N**. Monitoring Pathogen-Induced Sickness in Mice and Rats. *Curr Protoc Mouse Biol* 7: 65–76, 2017.

36. **Lee AY**, **Lee JW**, **Kim JE**, **Mock HJ**, **Park S**, **Kim S**, **Hong SH**, **Kim JY**, **Park EJ**, **Kang KS**, **Kim KP**, **Cho MH**. Dihydroceramide is a key metabolite that regulates autophagy and promotes fibrosis in hepatic steatosis model. *Biochem Biophys Res Commun* 494: 460–469, 2017.

37. **Leung K**, **Quezada M**, **Chen Z**, **Kanel G**, **Kaplowitz N**. Niacin-Induced Anicteric Microvesicular Steatotic Acute Liver Failure. *Hepatol Commun* 2: 1293–1298, 2018.

38. **Mansouri A**, **Gattolliat CH**, **Asselah T**. Mitochondrial Dysfunction and Signaling in Chronic Liver Diseases. *Gastroenterology* 155: 629–647, 2018.

39. **Marchais-Oberwinkler S**, **Henn C**, **Möller G**, **Klein T**, **Negri M**, **Oster A**, **Spadaro A**, **Werth R**, **Wetzel M**, **Xu K**, **Frotscher M**, **Hartmann RW**, **Adamski J**. 17β-Hydroxysteroid dehydrogenases (17β-HSDs) as therapeutic targets: Protein structures, functions, and recent progress in inhibitor development. *J Steroid Biochem Mol Biol* 125: 66–82, 2011.

40. **Matsuda M**, **Korn BS**, **Hammer RE**, **Moon YA**, **Komuro R**, **Horton JD**, **Goldstein JL**, **Brown MS**, **Shimomura I**. SREBP cleavage-activating protein (SCAP) is required for increased lipid synthesis in liver induced by cholesterol deprivation and insulin elevation. *Genes Dev* 15: 1206–1216, 2001.

41. **Moon YA**, **Horton JD**. Identification of two mammalian reductases involved in the two-carbon fatty

acyl elongation cascade. *J Biol Chem* 278: 7335–7343, 2003.

42. **Nagasaki S**, **Miki Y**, **Akahira J**, **Suzuki T**, **Sasano H**. Transcriptional regulation of 17beta-hydroxysteroid dehydrogenase type 12 by SREBP-1. [Online]. *Mol Cell Endocrinol* 307: 163–8, 2009. http://www.ncbi.nlm.nih.gov/pubmed/19533843 [5 Aug. 2019].

43. **Nagasaki S**, **Suzuki T**, **Miki Y**, **Akahira J -i.**, **Kitada K**, **Ishida T**, **Handa H**, **Ohuchi N**, **Sasano H**. 17 -Hydroxysteroid Dehydrogenase Type 12 in Human Breast Carcinoma: A Prognostic Factor via Potential Regulation of Fatty Acid Synthesis. *Cancer Res* 69: 1392–1399, 2009.

44. **Pietrocola F**, **Demont Y**, **Castoldi F**, **Enot D**, **Durand S**, **Semeraro M**, **Baracco EE**, **Pol J**, **Bravo-San Pedro JM**, **Bordenave C**, **Levesque S**, **Humeau J**, **Chery A**, **Métivier D**, **Madeo F**, **Maiuri MC**, **Kroemer G**. Metabolic effects of fasting on human and mouse blood in vivo. *Autophagy* 13: 567–578, 2017.

45. **Qi J**, **Lang W**, **Geisler JG**, **Wang P**, **Petrounia I**, **Mai S**, **Smith C**, **Askari H**, **Struble GT**, **Williams R**, **Bhanot S**, **Monia BP**, **Bayoumy S**, **Grant E**, **Caldwell GW**, **Todd MJ**, **Liang Y**, **Gaul MD**, **Demarest KT**, **Connelly MA**. The use of stable isotope-labeled glycerol and oleic acid to differentiate the hepatic functions of DGAT1 and -2. *J Lipid Res* 53: 1106–1116, 2012.

46. **Rantakari P**, **Lagerbohm H**, **Kaimainen M**, **Suomela JP**, **Strauss L**, **Sainio K**, **Pakarinen P**, **Poutanen M**. Hydroxysteroid (17β) dehydrogenase 12 is essential for mouse organogenesis and embryonic survival. *Endocrinology* 151: 1893–1901, 2010.

47. **Rautou PE**, **Cazals-Hatem D**, **Moreau R**, **Francoz C**, **Feldmann G**, **Lebrec D**, **Ogier-Denis É**, **Bedossa P**, **Valla D**, **Durand F**. Acute Liver Cell Damage in Patients With Anorexia Nervosa: A Possible Role of Starvation-Induced Hepatocyte Autophagy. *Gastroenterology* 135: 840–848, 2008.

48. **Rix**. Performance of severity parameters to detect chemotherapy-induced pain and distress in mice. 2019.

49. **Saha A**, **Biswas A**, **Srivastav S**, **Mukherjee M**, **Das PK**, **Ukil A**. Prostaglandin E 2 Negatively Regulates the Production of Inflammatory Cytokines/Chemokines and IL-17 in Visceral Leishmaniasis . *J Immunol* 193: 2330–2339, 2014.

50. **Sahu A**. Evidence suggesting that galanin (GAL), melanin-concentrating hormone (MCH), neurotensin (NT), proopiomelanocortin (POMC) and neuropeptide Y (NPY) are targets of leptin signaling in the hypothalamus. *Endocrinology* 139: 795–798, 1998.

51. **Sassmann A**, **Offermanns S**, **Wettschureck N**. Tamoxifen-inducible Cre-mediated recombination in adipocytes. *Genesis* 48: 618–625, 2010.

52. **Schwartz MW**, **Seeley RJ**, **Campfield LA**, **Burn P**, **Baskin DG**. Identification of targets of leptin action in rat hypothalamus. *J Clin Invest* 98: 1101–1106, 1996.

53. **Schwartz MW**, **Seeley RJ**, **Woods SC**, **Weigle DS**, **Campfield LA**, **Burn P**, **Baskin DG**. Leptin increases hypothalamic pro-opiomelanocortin mRNA expression in the rostral arcuate nucleus. *Diabetes* 46: 2119–2123, 1997.

54. **Scott HR**, **McMillan DC**, **Crilly A**, **McArdle CS**, **Milroy R**. The relationship between weight loss and interleukin 6 in non-small-cell lung cancer. *Br J Cancer* 73: 1560–1562, 1996.

55. **Senior JR**. Alanine aminotransferase: A clinical and regulatory tool for detecting liver injury-past, present, and future. *Clin Pharmacol Ther* 92: 332–339, 2012.

56. **Shrum B**, **Anantha R V.**, **Xu SX**, **Donnelly M**, **Haeryfar SMM**, **McCormick JK**, **Mele T**. A robust scoring system to evaluate sepsis severity in an animal model. *BMC Res Notes* 7: 1–11, 2014.

57. **Sokolović M**, **Sokolović A**, **Wehkamp D**, **van Themaat EVL**, **de Waart DR**, **Gilhuijs-Pederson LA**, **Nikolsky Y**, **van Kampen AHC**, **Hakvoort TBM**, **Lamers WH**. The transcriptomic signature of fasting murine liver. *BMC Genomics* 9: 1–20, 2008.

58. **Soriano P**. Generalized lacZ expression with the ROSA26 Cre reporter strain [1]. *Nat Genet* 21: 70–71, 1999.

59. **Spruss A**, **Henkel J**, **Kanuri G**, **Blank D**, **Püschel GP**, **Bischoff SC**, **Bergheim I**. Female mice are more susceptible to nonalcoholic fatty liver disease: sex-specific regulation of the hepatic AMP-activated protein kinase-plasminogen activator inhibitor 1 cascade, but not the hepatic endotoxin response. *Mol Med* 18: 1346–1355, 2012.

60. **Stekhoven DJ**, **Bühlmann P**. Missforest-Non-parametric missing value imputation for mixed-type data. *Bioinformatics* 28: 112–118, 2012.

61. **Szajnik M, Szczepanski MJ, Elishaev E, Visus C, Lenzner D, Zabel M, Glura M, DeLeo AB WT**. 17β hydroxysteroid dehydrogenase type 12 (HSD17B12) is a marker of poor prognosis in ovarian carcinoma. *Gynecol Oncol* 127: 587–594, 2012.

62. **Tanaka C**, **Asakawa A**, **Ushikai M**, **Sakoguchi T**, **Amitani H**, **Terashi M**, **Cheng KC**, **Chaolu H**, **Nakamura N**, **Inui A**. Comparison of the anorexigenic activity of CRF family peptides. *Biochem Biophys Res Commun* 390: 887–891, 2009.

63. **Velasco C**, **Librán-Pérez M**, **Otero-Rodiño C**, **López-Patiño MA**, **Míguez JM**, **Soengas JL**. Ceramides are involved in the regulation of food intake in rainbow trout (Oncorhynchus mykiss) . *Am J Physiol Integr Comp Physiol* 311: R658–R668, 2016.

64. **Venkatesan R**, **Sah-Teli SK**, **Awoniyi LO**, **Jiang G**, **Prus P**, **Kastaniotis AJ**, **Hiltunen JK**, **Wierenga RK**, **Chen Z**. Insights into mitochondrial fatty acid synthesis from the structure of heterotetrameric 3-ketoacyl-ACP reductase/3R-hydroxyacyl-CoA dehydrogenase. *Nat Commun* 5, 2014.

65. **Villanueva CJ**, **Monetti M**, **Shih M**, **Zhou P**, **Watkins SM**, **Bhanot S**, **Farese R V.** Specific role for acyl CoA:diacylglycerol acyltransferase 1 (Dgat1) in hepatic steatosis due to exogenous fatty acids. *Hepatology* 50: 434–442, 2009.

66. **Visus C**, **Ito D**, **Dhir R**, **Szczepanski MJ**, **Chang YJ**, **Latimer JJ**, **Grant SG**, **DeLeo AB**. Identification of Hydroxysteroid (17β) dehydrogenase type 12 (HSD17B12) as a CD8+ T-cell-defined human tumor antigen of human carcinomas. *Cancer Immunol Immunother* 60: 919–29, 2011.

67. **Vooijs M**, **Jonkers J**, **Berns A**. A highly efficient ligand-regulated Cre recombinase mouse line shows that [Online]. *Eur Mol Biol Organ* 2: 292–297, 2001. https://www.ncbi.nlm.nih.gov/pmc/articles/PMC1083861/pdf/kve064.pdf.

68. **Weil JG**, **Bains C**, **Linke A**, **Clark DW**, **Stirnadel HA**, **Hunt CM**. Background incidence of liver chemistry abnormalities in a clinical trial population without underlying liver disease. *Regul Toxicol Pharmacol* 52: 85–88, 2008.

69. **Wurie HR**, **Buckett L**, **Zammit VA**. Diacylglycerol acyltransferase 2 acts upstream of diacylglycerol acyltransferase 1 and utilizes nascent diglycerides and de novo synthesized fatty acids in HepG2 cells. *FEBS J* 279: 3033–3047, 2012.

70. **Yao X**, **Huang J**, **Zhong H**, **Shen N**, **Faggioni R**, **Fung M**, **Yao Y**. Targeting interleukin-6 in inflammatory autoimmune diseases and cancers. *Pharmacol Ther* 141: 125–139, 2014.

71. **Yao Z**, **Fanslow WC**, **Seldin MF**, **Rousseau AM**, **Painter SL**, **Comeau MR**, **Cohen JI**, **Spriggs MK**. Herpesvirus Saimiri encodes a new cytokine, IL-17, which binds to a novel cytokine receptor. *Immunity* 3: 811–821, 1995.

72. **Yao Z**, **Zhou H**, **Figeys D**, **Wang Y**, **Sundaram M**. Microsome-associated lumenal lipid droplets in the regulation of lipoprotein secretion. *Curr Opin Lipidol* 24: 160–170, 2013.

73. **Zambrowicz BP**, **Imamoto A**, **Fiering S**, **Herzenberg LA**, **Kerr WG**, **Soriano P**. Disruption of overlapping transcripts in the ROSA βgeo 26 gene trap strain leads to widespread expression of β-galactosidase in mouse embryos and hematopoietic cells. *Proc Natl Acad Sci U S A* 94: 3789–3794, 1997.

74. **Zhi X**, **Wang J**, **Lu P**, **Jia J**, **Shen H Bin**, **Ning G**. AdipoCount: A new software for automatic adipocyte counting. *Front Physiol* 9, 2018.

FIGURE LEGENDS

Figure 1. *Hsd17b12* expression, body weight and body composition in mice with induced HSD17B12 deletion at adulthood. (A) *Hsd17b12* expression in the liver, BAT, gonadal fat, adrenals, testis, thalamus, cerebral cortex, spleen, kidney, and colon of HSD17B12cKO male mice six days post induction, (Cre- lox/wt, Veh n=3-5; Cre- lox/wt, Tam n=3-6; Cre+ lox/lox, Veh n=4-5; Cre+ lox/lox, Tam n=4-6). Two liver samples of Cre- lox/wt were used as positive controls with every sample set and the expression level in them was set to 1. The expression levels in other tissues were proportioned to that of the positive controls. The results were analyzed with one-way ANOVA. (B) The body weight of HSD17B12cKO males and females decreased drastically within six days from the induction of Cre-recombination. Black circles: CTRL males (n=10-23), white circles: (KO) males (n=17-29), black squares: CTRL females (n=7-20), white squares: KO females (n=7-15). The CTRL (Cre- lox/wt, Tam) and KO (Cre+ lox/lox, Tam) groups in both sexes were compared with each other at each time point using t test. (C) *Top left:* Body fat mass. *Top right*: Lean mass. *Bottom left:* The ratio of fat mass to lean mass. *Bottom right:* Body water content of HSD17B12cKO mice on day six compared with the control mice. (Males Cre- lox/wt, Tam, n=6; males Cre+ lox/lox, Tam, n=7; females: Cre- lox/wt, Tam, n=7; females Cre+ lox/lox, Tam, n=6.) The CTRL (Cre- lox/wt, Tam) and KO (Cre+ lox/lox, Tam) groups in both sexes were compared with each other using t test. (D) Subcutaneous WAT and BAT depots of 10-week-old male mice were stained with PAS stain. *Top row*: Subcutaneous white fat and *bottom row*: Brown fat. Scale bar 100 μm.

Figure 2. Water and food consumption of HSD17B12cKO mice. (A) Cumulative water consumption of males during days three, four and five post induction. Two-way ANOVA. (B) Cumulative food consumption of males during days one to five post induction. Two-way ANOVA. (C) Lipid content in feces of control (CTRL) and HSD17B12cKO (KO) mice. (Males CTRL, Tam, n=3; males KO, Tam, n=4; females: CTRL, Tam, n=7; females KO, Tam, n=7). The CTRL and KO groups in both sexes were compared with each other using t test. (D) relative

mRNA expression levels of genes regulating hunger signaling [Neuropeptide Y (*Npy*) and Agouti-related peptide (*Agrp*)] as well as satiety signaling genes [proopiomelanocortin (*Pomc*) and Corticotropin releasing hormone (*Crh*)] in control (CTRL) and HSD17B12cKO (KO) female mice on day 6 post induction in the hypothalamus. T test. (CTRL, Cre- lox/lox, Tam, n=8; KO, Cre+ lox/lox, Tam, n=7-8).

Figure 3. Body composition of the adipocyte-specific HSD17B12cKO mice. (A) *Hsd17b12* expression in the liver, brown fat (BAT), gonadal fat (GF) and perirenal fat (RF) (Cre- lox/wt, Veh n=4; Cre- lox/wt, Tam n=4; Cre+ lox/lox, Veh n=4; Cre+ lox/lox, Tam n=5). One-way ANOVA. (B) Body weights of males and females. (C) The body fat mass of males and females, (D), lean mass, two-way ANOVA. (E) gonadal fat of five month old males stained with H&E and mean adipocyte size in gonadal fat of male mice (Cre- lox/wt, Veh n=3; Cre- lox/wt, Tam n=4; Cre+ lox/lox, Veh n=4; Cre+ lox/lox, Tam n=6). Scale bar=100μm. One-way ANOVA.

Figure 4. Serum lipidomics of HSD17B12cKO males on day six after tamoxifen induction. (A) Heatmap of lipid species concentration and (B) volcano plot of lipid class concentrations. (C) Lipid species composition of dihydroceramides (DCER), ceramides (CER), lactosylceramides (LCER) and hexosylceramides (HCER) of control (CTRL) and HSD17B12cKO (KO) males on day 6 post induction. T test. Gray lines represent median values. ND=not detected. (CTRL, Cre- lox/lox, Tam, n=5; KO, Cre+ lox/lox, Tam, n=5).

Figure 5. Liver histology of HSD17B12cKO males of 10 week-old male mice. Mice were sacrificed on day six after the induction of Cre-recombination. (A) Hematoxylin&Eosin (top row), Oil Red O (middle row) staining as well as terminal deoxynucleotidyl transferase dUTP nick end labeling of control (CTRL) and HSD17B12cKO (KO) male and female mice show microvesicular steatosis and apoptosis in the KO mice. The arrowheads indicate apoptotic cells and arrows indicate lipid droplets. (B) Alanine aminotransferase activity in serum, (C) the concentration of hepatic triglycerides, and (D) percentage of apoptotic cells in the liver on day six after Tam induction of control (CTRL) and HSD17B12cKO (KO) mice. Males CTRL, Cre- lox/lox, Tam, n=6-7 and KO, Cre+ lox/lox, Tam, n=6, females CTRL, Cre- lox/lox, Tam, n=5-6 and KO, Cre+ lox/lox, Tam, n=6-8. Squares

represent individual values and horizontal lines represent median value. Red squares indicate the animal seen in the histological images. T test. Scale bar 50 μm.

Figure 1

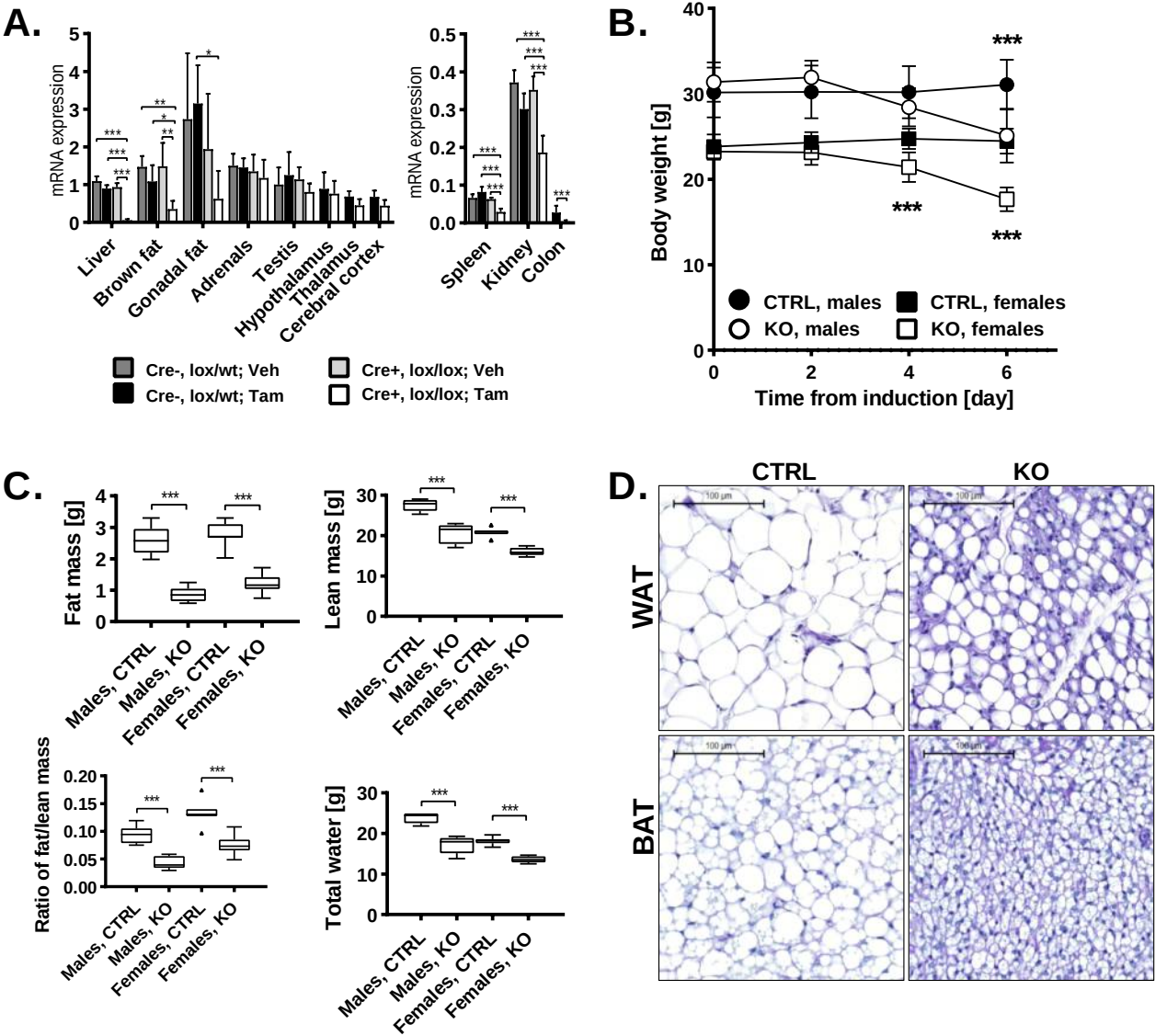
A.
mRNA expression
Liver
Brown fat
Gonadal fat
Adrenals
Testis
Hypothalamus
Thalamus
Cerebral cortex
Spleen
Kidney
Colon
Cre-, lox/wt; Veh
Cre-, lox/wt; Tam
Cre+, lox/lox; Veh
Cre+, lox/lox; Tam
B.
Body weight [g]
Time from induction [day]
CTRL, males
CTRL, females
KO, males
KO, females
C.
Fat mass [g]
Lean mass [g]
Ratio of fat/lean mass
Total water [g]
Males, CTRL
Males, KO
Females, CTRL
Females, KO
D.
CTRL
KO
WAT
BAT

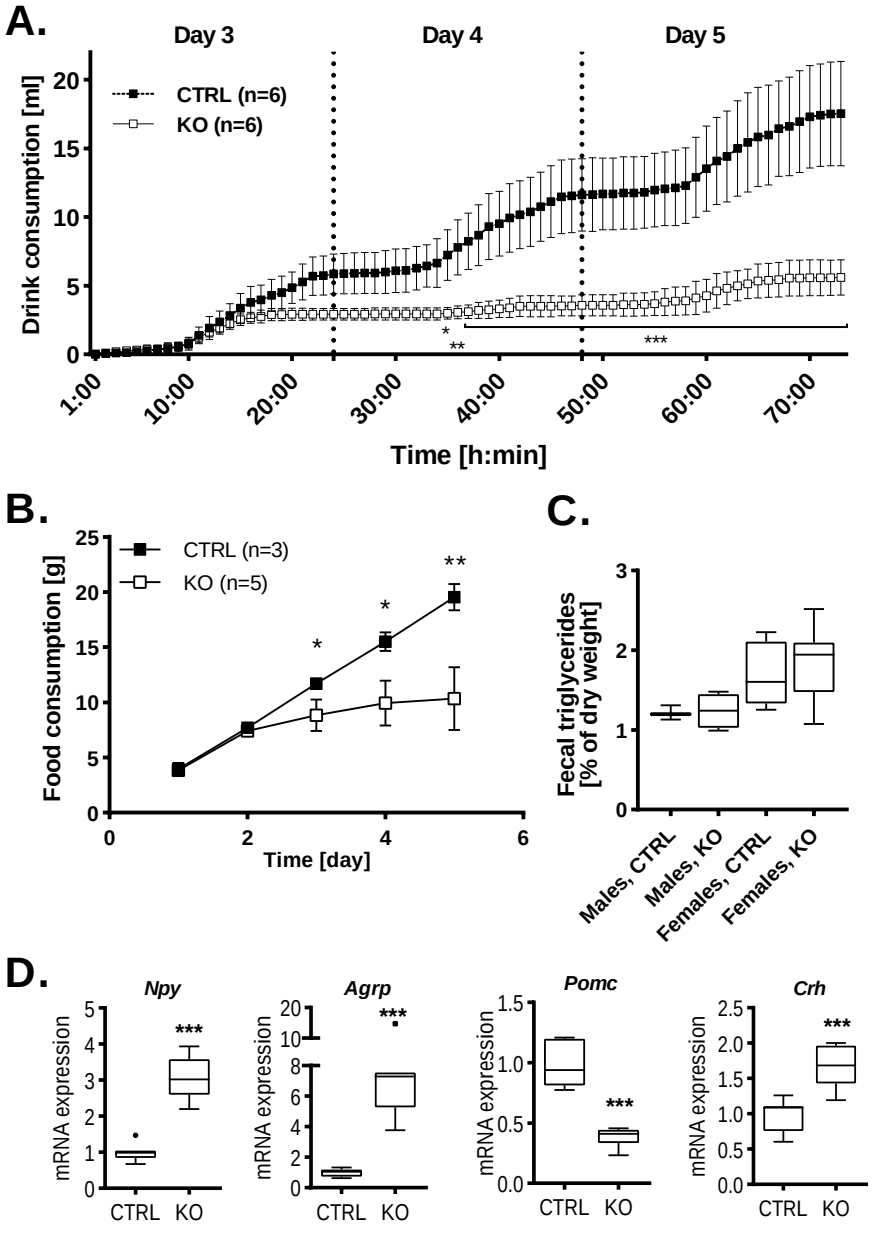
A.
Day 3
Day 4
Day 5
CTRL (n=6)
KO (n=6)
Drink consumption [ml]
Time [h:min]
B.
CTRL (n=3)
KO (n=5)
Food consumption [g]
Time [day]
C.
Fecal triglycerides [% of dry weight]
Males, CTRL
Males, KO
Females, CTRL
Females, KO
D.
Npy
Agrp
Pomc
Crh
mRNA expression
CTRL
KO

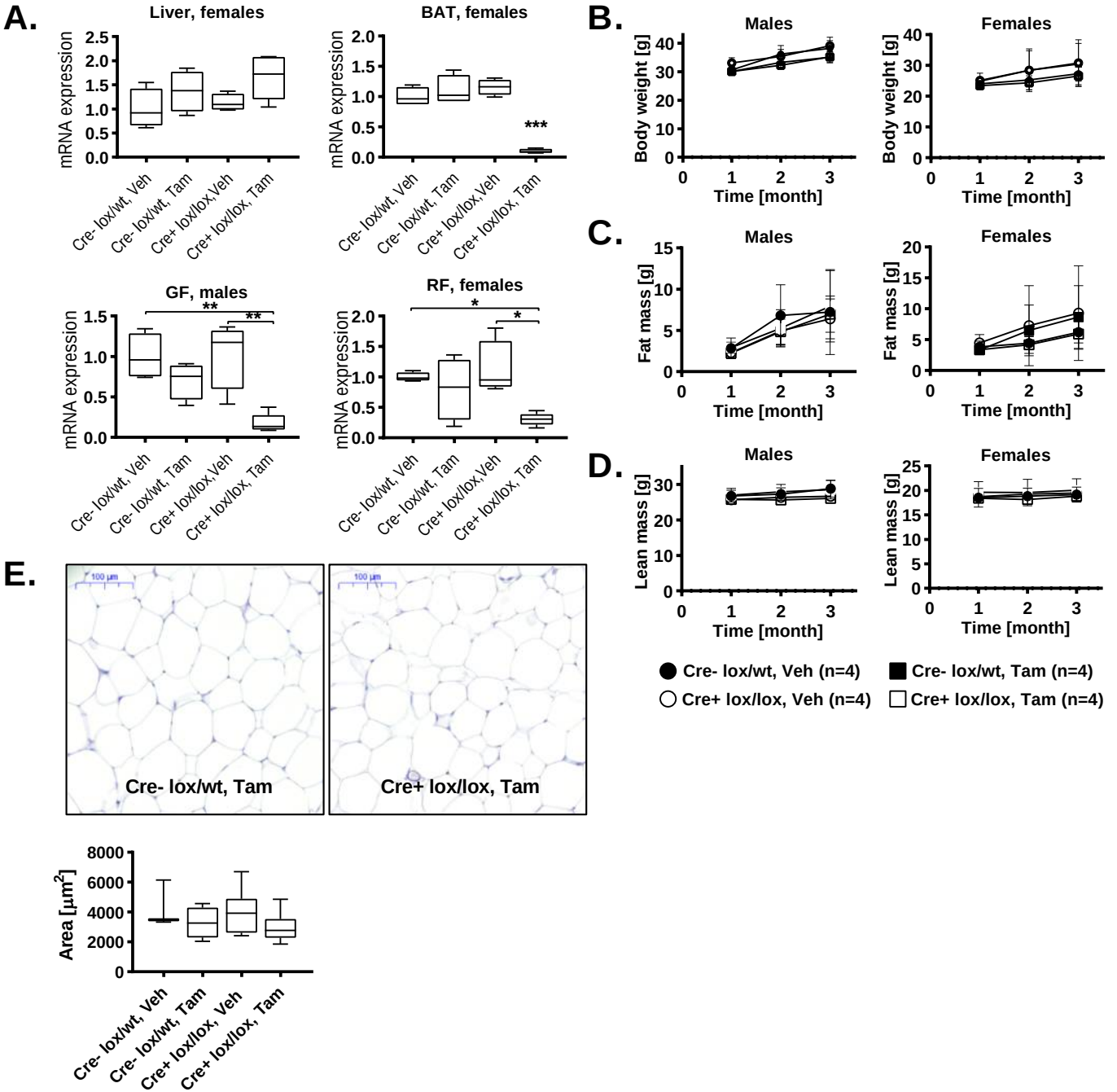
A.
Liver, females
BAT, females
GF, males
RF, females
mRNA expression
Cre- lox/wt, Veh
Cre- lox/wt, Tam
Cre+ lox/lox,Veh
Cre+ lox/lox, Tam
***
**
*
B.
Males
Females
Body weight [g]
Time [month]
C.
Fat mass [g]
D.
Lean mass [g]
Cre- lox/wt, Veh (n=4)
Cre- lox/wt, Tam (n=4)
Cre+ lox/lox, Veh (n=4)
Cre+ lox/lox, Tam (n=4)
E.
100 µm
Cre- lox/wt, Tam
Cre+ lox/lox, Tam
Area [µm²]

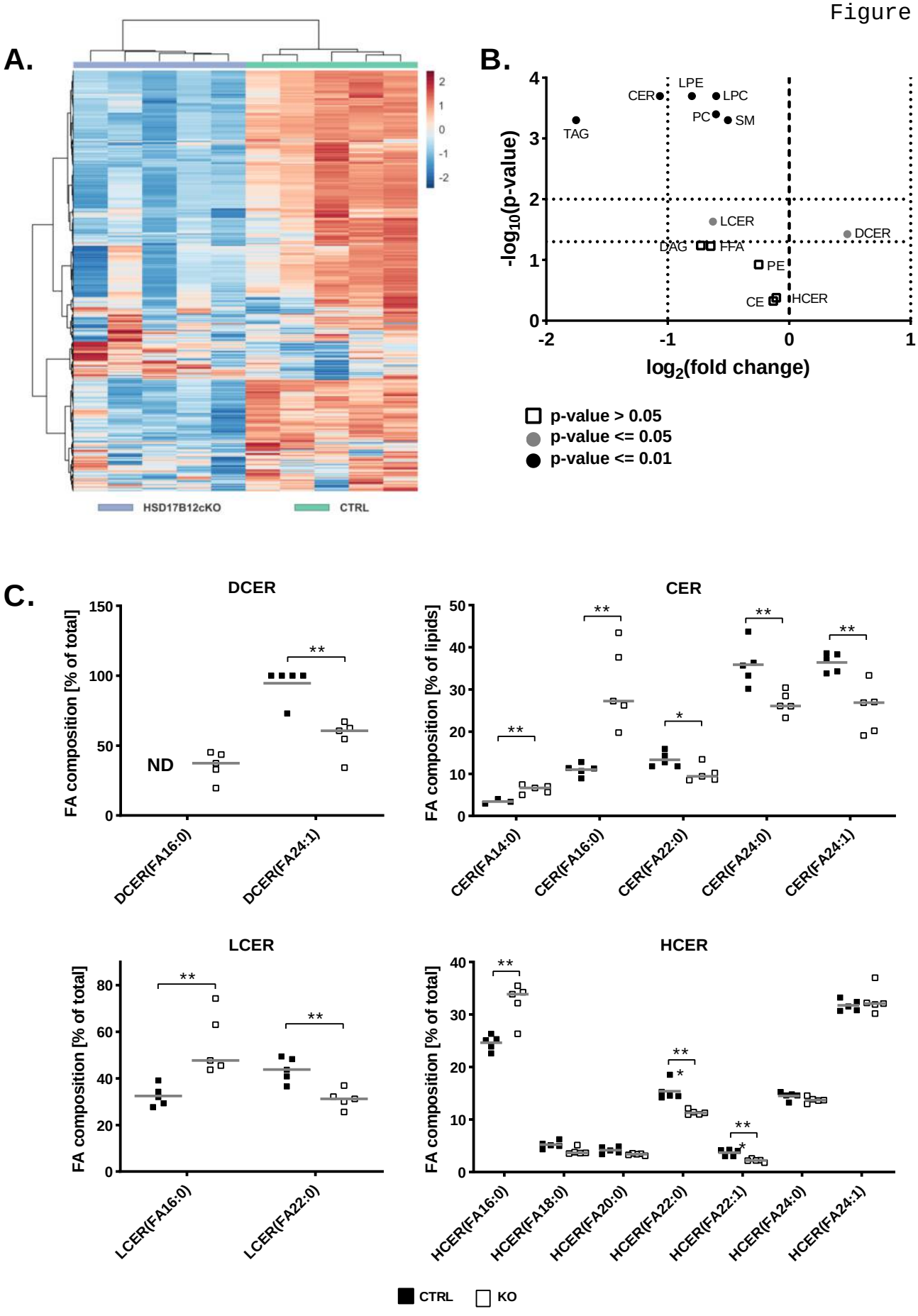
A.
2
1
0
-1
-2
HSD17B12cKO
CTRL
B.
LPE
CER
LPC
PC
SM
TAG
LCER
DCER
DAG
FFA
PE
CE
HCER
-log10(p-value)
log2(fold change)
p-value > 0.05
p-value <= 0.05
p-value <= 0.01
C.
DCER
FA composition [% of total]
ND
DCER(FA16:0)
DCER(FA24:1)
CER
FA composition [% of lipids]
CER(FA14:0)
CER(FA16:0)
CER(FA22:0)
CER(FA24:0)
CER(FA24:1)
LCER
FA composition [% of total]
LCER(FA16:0)
LCER(FA22:0)
HCER
FA composition [% of total]
HCER(FA16:0)
HCER(FA18:0)
HCER(FA20:0)
HCER(FA22:0)
HCER(FA22:1)
HCER(FA24:0)
HCER(FA24:1)
CTRL
KO

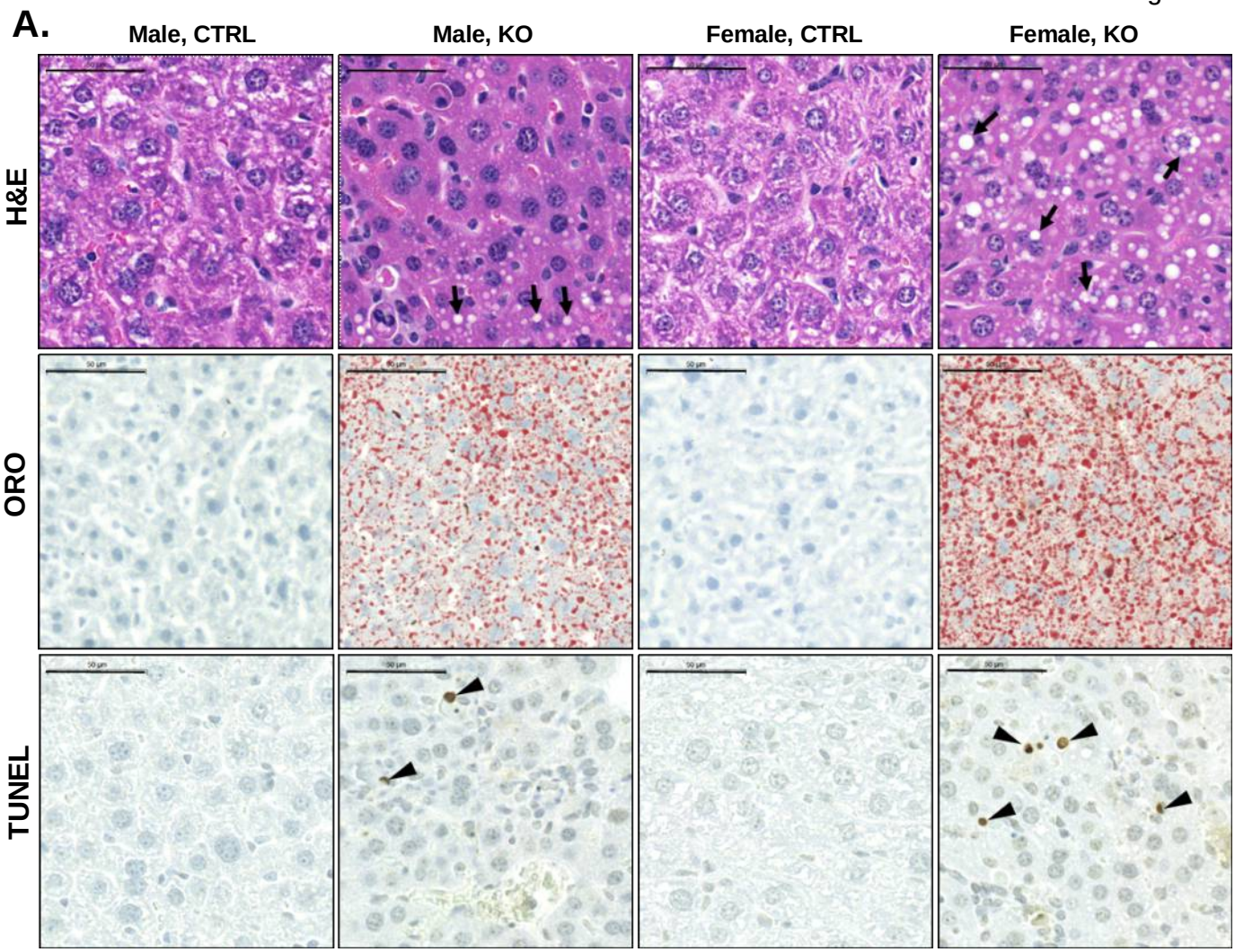
A.
Male, CTRL
Male, KO
Female, CTRL
Female, KO
H&E
ORO
TUNEL

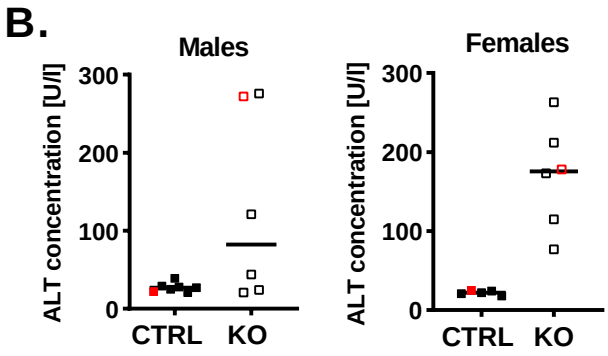
B.
Males
Females
ALT concentration [U/l]
300
200
100
0
CTRL
KO

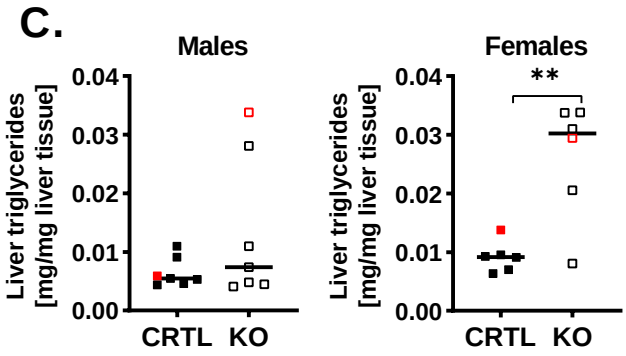
C.
Males
Females
Liver triglycerides [mg/mg liver tissue]
0.04
0.03
0.02
0.01
0.00
CRTL
KO
**

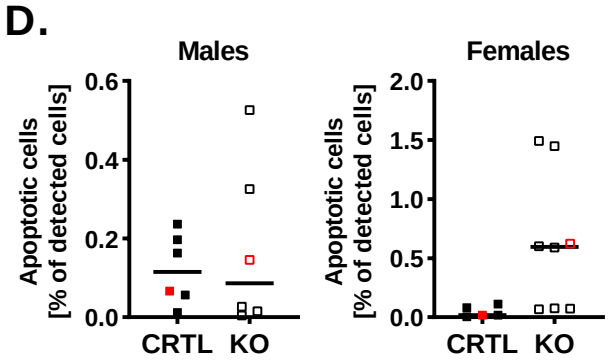
D.
Males
Females
Apoptotic cells [% of detected cells]
0.6
0.4
0.2
0.0
2.0
1.5
1.0
0.5
0.0
CRTL
KO

Table 1. Primers used for genotyping PCR and qRT-PCR assays.

Target		Sequence (5'- 3')	Amplicon size (bp)	Annealing T (C)
SCREENING PCR				
17bHSD12Arm5GF2	for	GCATGCTTCTCTTCTTTGTT	5314	55.0
17bHSD12Arm5UR1	rev	TACATAGTTGGCAGTGTTTG		
FRse1	for	GAGATGGCGCAACGCAATTA	4597	55.0
17HSD12Arm3GR2	rev	GCTGGAAAGGCTTTTGTGTC		
GENOTYPING PCR				
Hsd17b12	for	TTAGGCTTTACTAGCATATAGC	206 (wt)	60.0
	rev	TATAAGGAAACGGAAGCTCA	400 (loxP)	
Rosa26Cre	for	GCACGTTCACCGCATCAAC	320	60.0
	rev	CGATGCAACGAGTGATGAGGTTC		
Adipoq-Cre	for	ATACCGGAGATCATGCAAGC	200	58.0
	rev	GGCCAGGCTGTTCTTCTTAG		
qRT-PCR				
Acaca	for	GCCTCTTCCTGACAAACGAG	239	60.0
	rev	TGACTGCCGAAACATCTCTG		
Acox1	for	TTATGCGCAGACAGAGATGG	209	61.7
	rev	AGGCATGTAACCCGTAGCAC		
Agrp	for	CTTTGGCGGAGGTGCTAGAT	75	59.0
	rev	AGGACTCGTGCAGCCTTACAC		
CD36	for	GATGACGTGGCAAAGAACAG	107	59.6
	rev	TCCTCGGGGTCCTGAGTTAT		
Cpt1a	for	CCAGGCTACAGTGGGACATT	209	57.0
	rev	GAACTTGCCCATGTCCTTGT		
Crh	for	ACTCAGAGCCCAAGTACGTT	164	60.9
	rev	GCTCTCTTCTCCTCCCTTGG		
Dgat1	for	GCCACAATCATCTGCTTCCC	190	60.0
	rev	CCACTGACCTTCTTCCCTGT		
Dgat2	for	CCAAGAAAGGTGGCAGGA	174	60.0
	rev	TGAAGTTACAGAAGGCACCC		
Fasn	for	TGGGTTCTAGCCAGCAGAGT	158	59.0
	rev	ACCACCAGAGACCGTTATGC		
Fatp2	for	ATGCCGTGTCCGTCTTTTAC	168	59.6
	rev	GACCTGTGGTTCCCGAAGTA		
G6pc	for	CTGTTTGGACAACGCCCGTAT	91	61.8
	rev	AGGTGACAGGGAACTGCTTTA		
L19	for	GGACAGAGTCTTGATGATCTC	195	60.0
	rev	CTGAAGGTCAAAGGGAATGTG		
Npy	for	CCGCTCTGCGACACTACAT	68	60.9
	rev	TGTCTCAGGGCTGGATCTCT		
Pepck	for	CTGAAGGTGTCCCCCTTGTC	110	59.6
	rev	GATCTTGCCCTTGTGTTCTGC		
Pklr	for	TGGCATCGAAAGTGGAAAGC	193	60.9
	rev	GATGTGGGACTATGGGAGGG		
Pomc	for	CAAGCCGGTGGGCAAGAAACG	119	60.9
	rev	CTAATGGCCGCTCGCCTTCCAG		
Ppara	for	ATGCCAGTACTGCCGTTTTC	220	61.8
	rev	GGCCTTGACCTTGTTCATGT		
Ppia	for	CATCCTAAAGCATACAGGTCCTG	165	60.0
	rev	TCCATGGCTTCCACAATGTT		
Scd1	for	CATTCTCATGGTCCTGCTGC	163	59.6
	rev	TGCCTTGTAAGTTCTGTGGC		

for=forward, rev=reverse, bp=base pairs

Table 2. Clinical chemistry results from whole blood of HSD17B12cKO mice.

	Males				Females			
Parameter	**Control n=7**	**HSD17B12cKO n=6**	**Fold Change**	**p-value**	**Control n=5**	**HSD17B12cKO n=5**	**Fold Change**	**p-value**
Albumin (g/l)	40.7 ± 2.43	46.8 ± 3.49	1.15	0.017*	46.2 ± 1.30	50.8 ± 3.06	1.10	0.013*
Alkaline phosphatase (U/l)	134 ± 25.1	186 ± 37.5	1.39	0.024*	198 ± 23.4	180 ± 27.4	0.91	0.429
Alanine aminotransferase (U/l)	27.3 ± 5.96	126 ± 120	4.63	0.190	22.0 ± 2.73	170 ± 66.6	7.71	0.004**
Amylase (U/l)	827 ± 52.9	870 ± 163	1.05	0.485	715 ± 34.4	653 ± 144	0.91	0.429
Total bilirubin (µmol/l)	4.57 ± 0.79	4.80 ± 0.84	1.05	0.665	4.40 ± 0.54	5.00 ± 1.00†	1.14	0.357
Blood urea nitrogen (mmol/l)	7.66 ± 0.69	14.1 ± 14.3	1.84	0.394	6.84 ± 1.08	15.2 ± 13.9	2.23	0.011*
Total calcium (mmol/l)	2.51 ± 0.05	2.52 ± 0.08	1.01	0.732	2.56 ± 0.04	2.62 ± 0.03	1.02	0.050*
Phosphate (mmol/l)	2.95 ± 0.45	2.03 ± 0.46	0.69	0.026*	2.37 ± 0.36	2.31 ± 0.44	0.98	0.931
Creatinine (µmol/l)	23.1 ± 5.58	29.3 ± 11.6	1.27	0.446	25.6 ± 7.76	22.5 ± 7.15	0.88	0.307
Glucose (mmol/l)	8.71 ± 1.55	5.33 ± 3.24	0.61	0.071	8.12 ± 1.36	5.13 ± 2.00	0.63	0.017*
Sodium (mmol/l)	148 ± 1.89	149 ± 2.40	1.01	0.316	148.± 2.68	154 ± 3.44	1.04	0.022*
Potassium (mmol/l)	6.26 ± 0.81	5.78 ± 0.67	0.92	0.452	5.90 ± 1.13	6.23 ± 1.19†	1.06	0.875
Total protein (g/l)	58.1 ± 2.54	65.7 ± 5.72	1.13	0.039*	60.2 ± 1.64	66.3 ± 4.97	1.10	0.015*
Globulins (g/l)	17.1 ± 2.19	18.8 ± 2.56	1.10	0.290	14.0 ± 0.71	15.7 ± 2.73	1.12	0.221

Stars indicate significantly different results

Table 3. Cytokine concentrations measured in serum of HSD17B12cKO mice.

	Males				Females			
Cytokine	**Control n=10**	**HSD17B12cKO n=10**	**FC**	**p-value**	**Control n=9**	**HSD17B12cKO n=10**	**FC**	**p-value**
G-CSF	511 ± 266	1175 ± 299	2.30	<0.001 ***	628 ± 341	7953 ± 3753	12.6	<0.001 ***
IFN-y	5.32 ± 2.02	4.38 ± 1.59	-1.22	ns	6.10 ± 2.86	3.86 ± 2.36	-1.58	0.028 *
IL-1a	417 ± 104	279 ± 87.9	-1.50	0.005 **	228 ± 74.2	199 ± 114	-1.15	ns
IL-5	23.7 ± 17.6	10.0 ± 3.56	-2.37	0.009 **	27.2 ± 6.29	20.9 ± 16.5	-1.30	ns
IL-6	7.43 ± 7.90	59.6 ± 48.9	8.02	<0.001 ***	5.35 ± 1.37	189 ± 125	35.3	<0.001 ***
IL-17	20.44 ± 9.74	117.5 ± 96.2	5.75	0.005 **	35.75 ± 27.0	147.9 ± 88.1	4.14	0.001 **
IP-10	481 ± 116	353 ± 121	-1.36	0.026 *	391 ± 100	409 ± 209	1.05	ns
KC	710 ± 496	531 ± 477	-1.34	ns	385 ± 186	1756 ± 1040	4.55	0.002 **
MIP-1a	32.1 ± 12.1	39.7 ± 20.3	1.24	ns	32.1 ± 8.87	20.9 ± 5.84	-1.54	0.014 *

Mean ± SD. T test or nonparametric Mann-Whitney test depending on the normality of the data. Stars indicate significantly different results. FC= Fold change. ns=not significant

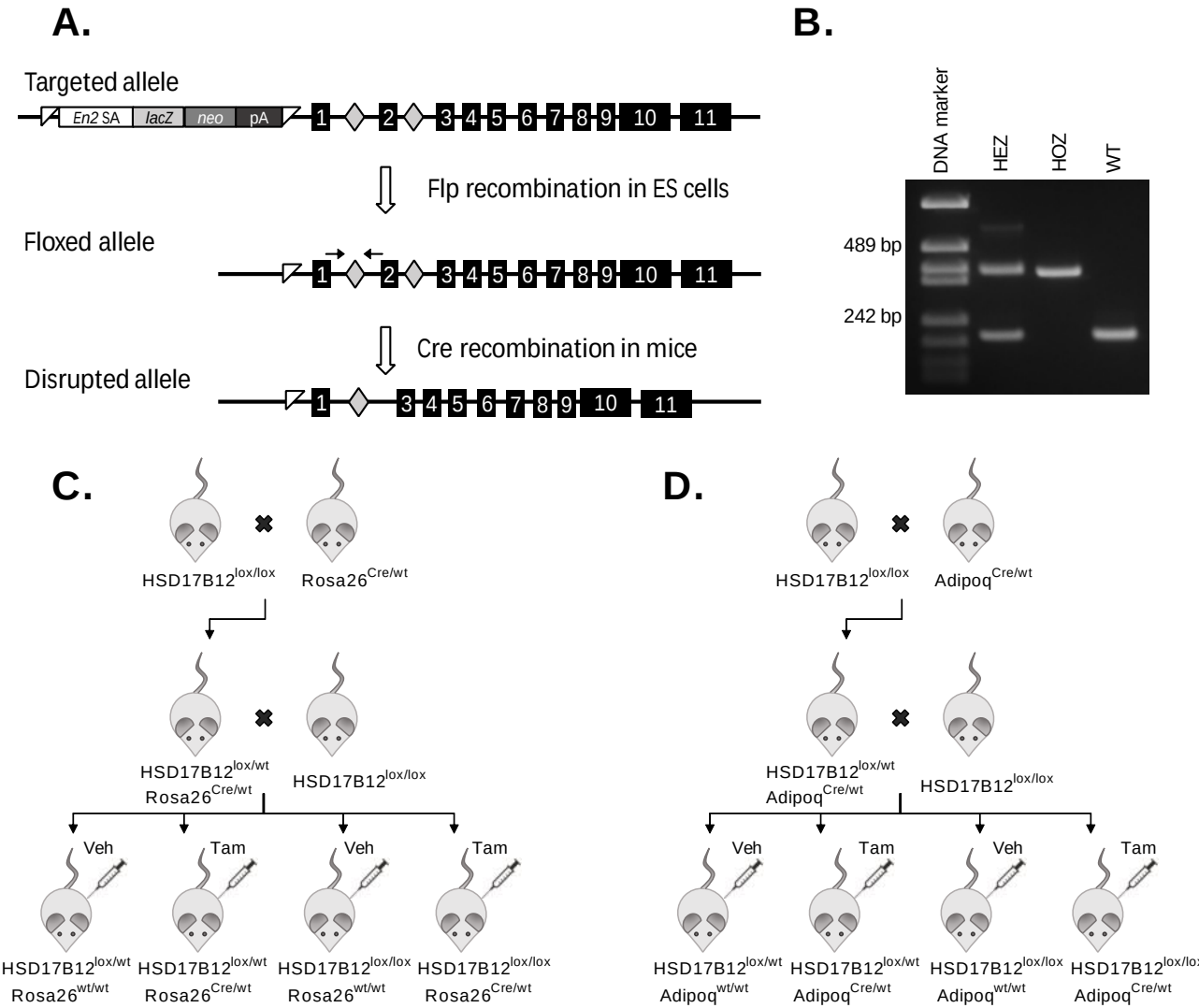

Supplemental Figure S1. Generation of the conditional HSD17B12 knockout mice. (A) The triangles represent *FRT* sequences, the diamonds represent *loxP* sequences, the black arrows represent genotyping primer annealing sites, and the black boxes represent exons. The promoterless cassette consisted of *engrailed-2* splice acceptor (*En2* SA), β-galactosidase coding *LacZ* sequence (*lacZ*), the neomycin resistance gene (*neo*) and polyadenylation signal (pA). (B) Genotyping image of the HSD17B12-loxP mouse strain (HEZ=heterozygous, HOZ= homozygous). (C) and (D) schematic representations of the breeding to generate the mice in which the gene disruption was induced by Tam treatment to produce the HSD17B12cKO and adipocyte-specific aHSD17B12cKO mouse strains.

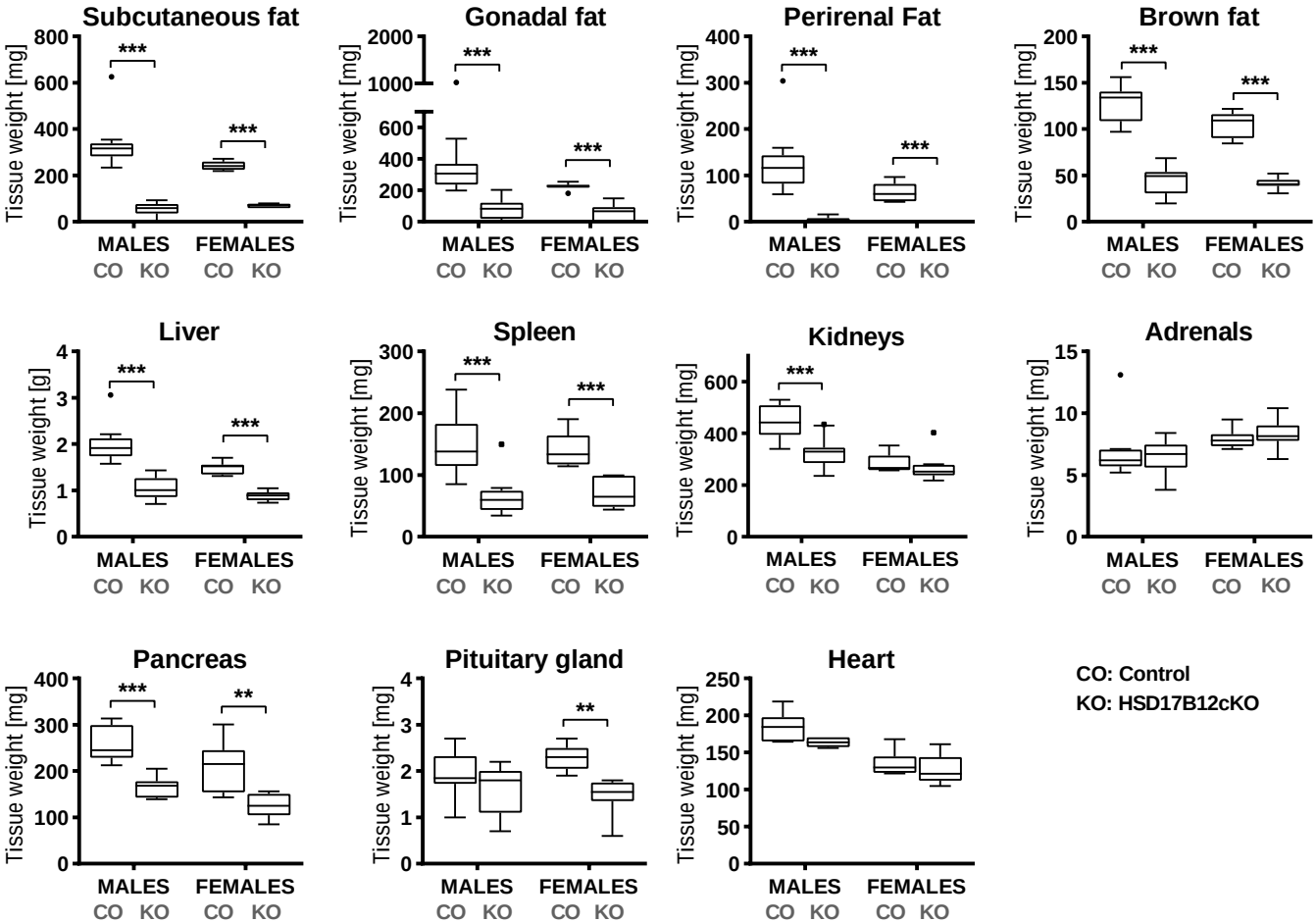

Supplemental Figure S2. Internal organ weights on day six after tamoxifen induction in HSD17B12cKO (KO; Cre+ lox/lox, Tam) and controls (CO; Cre- lox/lox, Tam). Males CO n=12, males KO n=13, females CO n=7 and females KO n=7, except in liver males CO n=13, males KO n=14, females CO n=13 and females KO n=15. T test.

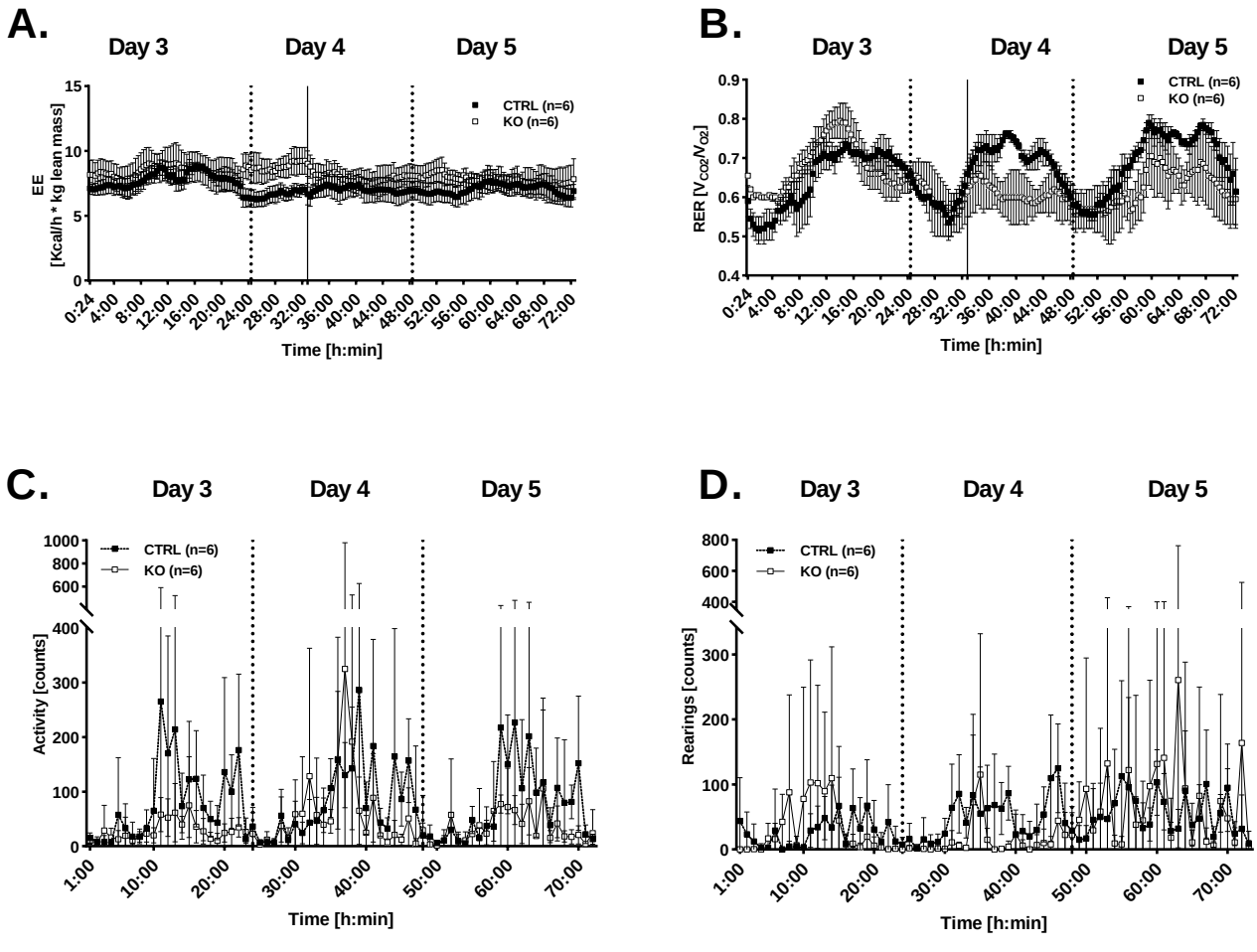

Supplemental Figure S3. Energy expenditure, respiratory exchange ratio and activity of HSD17B12cKO males 3 to 5 days post induction. (A) The energy expenditure of HSD17B12cKO (KO; Cre+ lox/lox, Tam) mice does not differ that of control mice (CTRL; Cre- lox/lox, Tam). (B) The respiratory exchange ratio of the males becomes lower during day 4 post-induction. The solid vertical line indicates the beginning point of switching from carbon to fat as an energy fuel in the HSD17B12cKO males. (C) The locomotor activity and (D) rearing events did not differ between the KO and control mice. Two way ANOVA.

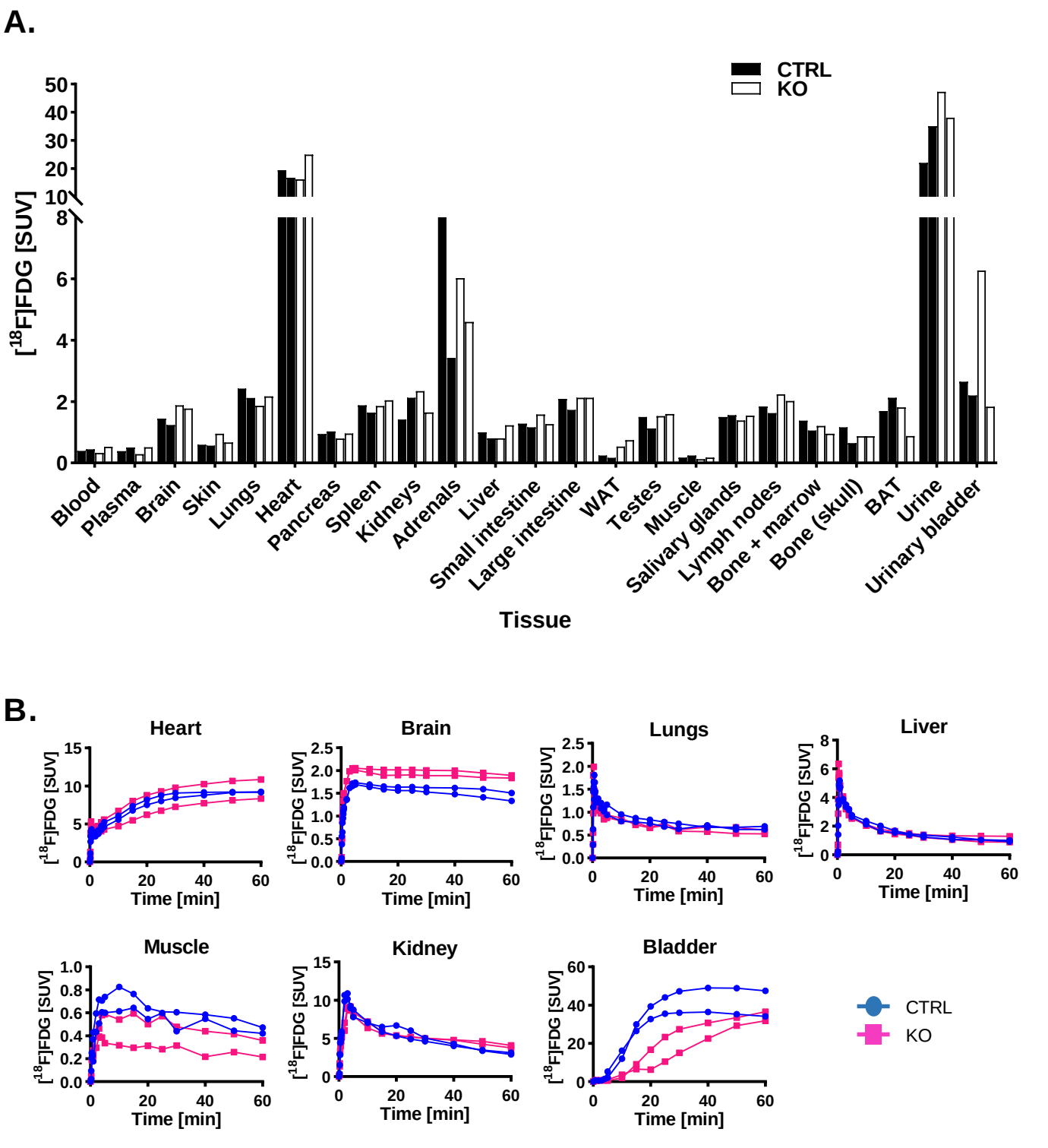

Supplemental Figure S4. Effects of *Hsd17b12* disruption on glucose uptake (A) *Ex vivo* biodistribution of [^{18}F]FDG uptake over 60 minutes on day five post-induction in control (CTRL; Cre- lox/lox, Tam) and HSD17B12cKO (KO; Cre+ lox/lox, Tam) mice. Each bar represents one mouse. (B) Time-activity curves of various tissues obtained from PET imaging on day 5 post induction. Each line represents one mouse. SUV=standardized uptake unit.

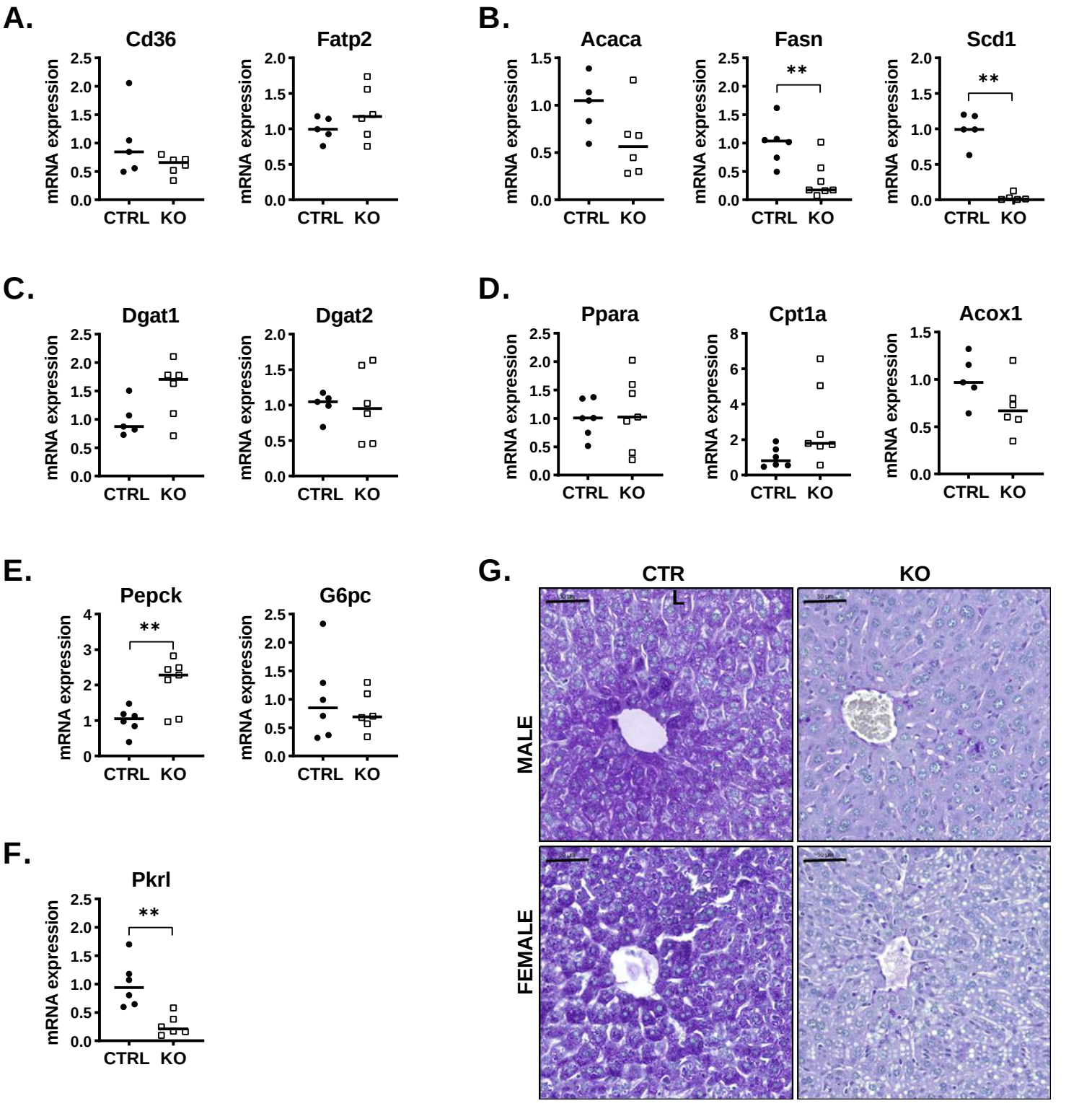

Supplemental Figure S5. Gene expression of key metabolic pathways in the liver on day six after Tam induction in control and KO male mice by qPCR. (A) mRNA expression of genes related to FA uptake, (B) *de novo* lipogenesis (C) FA esterification, (D) FA oxidation (E) glukoneogenesis and (F) glycolysis. (G) Periodic acid–Schiff staining of male and female livers on day six after Tam induction. T test or Mann-Whitney test. Squares represent individual values and horizontal lines represent median values. Scale bar 50 μm.